Nonlinear Trivelpiece-Gould waves: Frequency, functional form, and stability

D. H. E. Dubin and A. Ashourvan
Department of Physics, UCSD, La Jolla, California 92093, USA

(Received 10 August 2015; accepted 14 September 2015; published online 6 October 2015)

This paper considers the frequency, spatial form, and stability of nonlinear Trivelpiece-Gould (TG) waves on a cylindrical plasma column of length L and radius r_p, treating both traveling waves and standing waves, and focussing on the regime of experimental interest in which $L/r_p \gg 1$. In this regime, TG waves are weakly dispersive, allowing strong mode-coupling between Fourier harmonics. The mode coupling implies that linear theory for such waves is a poor approximation even at fairly small amplitude, and nonlinear theories that include a small number of harmonics, such as three-wave parametric resonance theory, also fail to fully capture the stability properties of the system. It is found that nonlinear standing waves suffer jumps in their functional form as their amplitude is varied continuously. The jumps are caused by nonlinear resonances between the standing wave and nearly linear waves whose frequencies and wave numbers are harmonics of the standing wave. Also, the standing waves are found to be unstable to a multi-wave version of three-wave parametric resonance, with an amplitude required for instability onset that is much larger than expected from three wave theory. It is found that traveling waves are linearly stable for all amplitudes that could be studied, in contradiction to three-wave theory. © *2015 AIP Publishing LLC*.
[http://dx.doi.org/10.1063/1.4932001]

I. INTRODUCTION

In this paper, we consider the theory of nonlinear Trivelpiece-Gould (TG) waves on a cylindrical cold plasma column. These plasma waves have been studied in theory and in experiments spanning several decades of research,[1–5] and their nonlinear behavior has recently received renewed attention.[6,7] Their linear dispersion relation is also similar to that of cold magnetized plasma waves in a uniform plasma, ion acoustic waves,[8] and shallow water waves in the Boussinesq approximation, the nonlinear behavior of which has been extensively studied.[9]

Here, we construct nonlinear solutions for both traveling and standing TG waves, focussing on the regime of current experimental interest, $L/r_p \gg 1$, where L and r_p are the plasma column length and radius, respectively. The traveling waves are described using periodic boundary conditions, and the standing waves are described with Neumann conditions appropriate to the experiments. In the regime $L/r_p \gg 1$, these waves are only weakly dispersive. Consequently, these TG waves display strong nonlinear effects even at small amplitude. For a system with weak dispersion, a harmonic of a finite amplitude wave, with a frequency and wavenumber that are a given multiple of the fundamental, is nearly on the linear dispersion relation themselves and consequently is driven resonantly to large amplitude by the fundamental, through nonlinear mode coupling. This implies that linear theory is a poor approximation for such waves, even at small amplitudes, and also that nonlinear theories that incorporate only a few harmonics, such as perturbation theory, or the theory of three-wave parametric resonance, are of limited usefulness.

The traveling-wave solutions that we construct display a strong positive nonlinear frequency shift with increasing amplitude, up to a maximum amplitude associated with the formation of a stagnation point in the fluid flow. Soliton solutions are also found, with the usual K-dV functional form at low amplitude[10,11] and a more strongly peaked form at larger amplitudes. For standing waves, we observe a novel behavior: apparently discontinuous jumps in the functional form of the standing wave solutions as amplitude is varied. The jumps have the appearance of a nonlinear resonance, in which a high-order Fourier mode in the solution becomes excited, producing a ripple whose amplitude increases as the resonance is approached, and then switches phase by 180° across the resonance. In fact, each observed jump can be correlated to a degeneracy between the amplitude-dependent nonlinear standing wave frequency and a nearly linear wave that has given multiples of the standing wave frequency and wavenumber. These waves are resonantly excited by the standing wave because it contains many harmonics of the fundamental in both space and time.

We then analyze the linear stability of these waves with respect to small perturbations of the nonlinear waveform. An oft-used model of instability is reviewed: three-wave parametric resonance, in which a nonlinear wave (termed the pump wave in three wave theory) interacts with two longer-wavelength "daughter waves."[12–15] When a resonance condition is met, the daughter waves can be driven unstable by the pump wave. Such parametric resonances are observed in many nonlinear systems, including TG waves. In fact, several aspects of the observations of the nonlinear TG wave instability can be fitted by the three-wave model.[6]

However, the actual system is not confined to only three waves. Neither the nonlinear pump wave nor the growing daughter waves are single Fourier modes, as is assumed in three wave theory. Even at moderate amplitudes, mode-coupling produces many Fourier harmonics in the nonlinear waves, which have a strong effect on their stability,

particularly for $L/r_p \gg 1$. When the correct form of the pump and daughter waves is used, keeping multiple Fourier harmonics in each, we find that the system is far less unstable than three wave theory would predict.

For nonlinear traveling waves, we find that the solutions are stable for all amplitudes we could consider with the Fourier method employed in this paper. For standing waves, we find that there is a range of amplitudes which are unstable, depending on the parameters of the TG dispersion relation, in particular, the perpendicular wavenumber $k_\perp$, a parameter in the dispersion relation proportional to $1/r_p$. However, the amplitude required for instability onset is much larger than predicted by three-wave theory, particularly for $k_\perp L \gg 1$, and the calculated growth rate is smaller.

In Section II, we introduce the fluid equations used to describe TG waves. In Section III, we analyze the functional form and frequency of nonlinear traveling TG waves using two methods: a direct integration of the differential equations in Sec. III A, and a Fourier expansion of the solution in Sec. III B. In Sec. III B 1, we analyze the form of the nonlinear wave and the wave phase velocity in a small amplitude perturbation expansion. In Section IV, we analyze the functional form of nonlinear standing waves using a Fourier expansion and consider the small amplitude limit as a perturbation expansion. In Section V A, we consider the linear stability of traveling waves, and in Section V B we examine the stability of standing waves, using both three wave theory and the more general M-wave theory. Results and open questions are discussed in Sec. VI. Appendix A contains a brief analysis of the $k_\perp = 0$ limit of the equations, and Appendix B describes the method employed in our nonlinear simulations of the TG system.

II. MODEL

We consider nonlinear magnetized Langmuir (Trivelpiece-Gould) waves in a cold but collisionless homogeneous plasma column with radius r_p, length L, and uniform equilibrium density n_0. The plasma column is held inside a conducting cylinder of radius r_w by a strong uniform magnetic field in the z direction (along the axis of the column). Neglecting cyclotron motion and cross-magnetic field drifts, particles move only in the z direction in response to the electrostatic field of the wave. We use cold fluid theory to describe the plasma motion and concentrate on azimuthally symmetric modes. The plasma density n, fluid velocity v, and electrostatic potential ϕ are then functions only of time t, axial position z, and cylindrical radius r. The cold fluid equations of motion for these three functions are

$$\frac{\partial n}{\partial t} + \frac{\partial}{\partial z}(nv) = 0, \tag{1}$$

$$\frac{\partial v}{\partial t} + v\frac{\partial v}{\partial z} = -\frac{\partial \phi}{\partial z}, \tag{2}$$

$$\frac{1}{r}\frac{\partial}{\partial r}\left(r\frac{\partial \phi}{\partial r}\right) + \frac{\partial^2 \phi}{\partial z^2} = -n, \tag{3}$$

where for simplicity all quantities are dimensionless: density is normalized to the (constant) equilibrium density n_0, distance is normalized by the fundamental axial wavenumber of the plasma column $k_1 = \pi/L$, time is normalized to the plasma frequency $\sqrt{4\pi e^2 n_0/m}$, velocity is normalized to ω_p/k_1, and electrostatic potential to $m\omega_p^2/ek_1^2$.

Equations (1)–(3) form a closed set, amenable to numerical and analytical study. However, radial dependence and finite plasma length effects in the equations are complicating factors. To simplify, we further assume that the plasma is a long thin column and neglect end effects, taking periodic boundary conditions with period $2L$.[16,17] We also simplify by integrating over the radial dependence using the following argument.[3] We concentrate on nonlinear plasma modes with no radial nodes (i.e., the lowest radial standing mode). For these modes, low amplitude (linear) perturbations to the equilibrium have a Bessel function radial dependence within the plasma, described as

$$\begin{aligned} n(r,z,t) &= 1 + J_0(k_\perp r)\delta n(z,t), \\ v(r,z,t) &= J_0(k_\perp r)\delta v(z,t), \\ \phi(r,z,t) &= \phi_0(r) + J_0(k_\perp r)\delta\phi(z,t), \end{aligned} \tag{4}$$

where $\phi_0(r)$ is the equilibrium plasma potential, $k_\perp$ is the (scaled) perpendicular wavenumber, given by

$$k_\perp^2 = \frac{2}{\bar{r}_p^2 \ln(r_w/r_p)}, \tag{5}$$

and $\bar{r}_p = k_1 r_p$ is the scaled plasma radius. Equation (5) is valid provided that $L/r_w \gg 1$. (A more general expression for $k_\perp$ can be found in Ref. 18.) Approximate nonlinear equations may then be obtained by substituting Eqs. (4) into Eqs. (1)–(3) and integrating over radius out to r_p. This simplification neglects nonlinear mixing of different radial modes.[3] The result is a set of nonlinear equations

$$\frac{\partial N}{\partial t} + \frac{\partial}{\partial z}(NV) = 0, \tag{6}$$

$$\frac{\partial V}{\partial t} + V\frac{\partial V}{\partial z} = -\frac{\partial \Phi}{\partial z}, \tag{7}$$

$$\frac{\partial^2 \Phi}{\partial z^2} - k_\perp^2 \Phi = 1 - N, \tag{8}$$

where $N(z,t)=1+\beta\delta n(z,t), V(z,t)=\beta\delta v(z,t), \Phi(z,t)=\beta\delta\phi(z,t)$, and

$$\begin{aligned} \beta &= \left(2/\bar{r}_p^2\right)\int_0^{\bar{r}_p} r dr J_0(k_\perp r) = \frac{2}{k_\perp \bar{r}_p} J_1(k_\perp \bar{r}_p) \\ &\sim 1 - k_\perp^2 \bar{r}_p^2/8, \ k_\perp \bar{r}_p < 1, \end{aligned} \tag{9}$$

is a scaling factor. (Somewhat different scaling factors can be obtained depending on how one defines the radial average.) Equations (6)–(8) are identical to those found in Ref. 3 except that here we keep the second derivative in z of the potential in the Poisson equation as it provides the (weak) dispersion necessary for the existence of nonlinear periodic solutions. For low (but not infinitesimal) amplitudes, these equations have been previously shown to have soliton

solutions identical to those of the K-dV equation.[11] Similar equations have also been studied in other contexts. For example, if one replaces the Poisson equation (8) by

$$\frac{\partial^2\Phi}{\partial z^2} = \exp(\Phi) - N, \tag{10}$$

one has a model for nonlinear ion sound waves.[20] If one instead drops Eq. (8) and replaces Eq. (7) by

$$\frac{\partial V}{\partial t} + V\frac{\partial V}{\partial z} = -k_\perp^{-2}\frac{\partial}{\partial z}\left(N + \frac{\partial^2 N}{\partial t^2}\right), \tag{11}$$

one obtains a well-known form of the Boussinesq equations describing slightly dispersive nonlinear shallow water waves.[19] Both these models have the same linear dispersion relation as Eqs. (6)–(8)

$$\omega^2 = m^2/(m^2 + k_\perp^2), \tag{12}$$

(with $k_\perp = 1$ in the ion sound wave model), where perturbations for linear mode m have (unscaled) axial wavenumber $k_m = mk_1$.

The $k_\perp = 0$ form of Eqs. (6)–(8) describes unmagnetized Langmuir waves in a cold $1D$ plasma. This well-studied system[21] admits a general nonlinear analytic solution in Lagrangian coordinates. It is highly degenerate, with all initial perturbations oscillating at the plasma frequency (as seen in a frame where the mean plasma velocity is zero), independent of spatial form or amplitude, provided that the amplitude is sufficiently small so that characteristics do not cross. This case is discussed briefly in Appendix A. The finite temperature extension of this system has also been closely studied, as it exhibits a self-focussing instability termed "Langmuir collapse."[22]

Here, we focus on the zero-temperature $k_\perp > 1$ regime of interest in experiments on TG waves. We construct fully nonlinear traveling and standing wave solutions to Eqs. (6)–(8). We then study the stability of these solutions, focusing on instability due to 3-wave parametric resonance. It is necessary to go beyond the small-amplitude K-dV version of the equations in order to study parametric instability, because we will see that onset of the instability only occurs (when it occurs at all) for large amplitudes with $N - 1 \approx O(1)$.

III. TRAVELING WAVE SOLUTIONS

In this section, we construct nonlinear traveling-wave solutions of our model equations (6)–(8) using two methods. Both methods use the standard traveling-wave ansatz whereby functions of t and z are assumed to depend only on the combination $z - ut \equiv s$, where u is the velocity of the nonlinear wave. In what follows, we assume that $u > 0$ (the traveling wave moves to the right). This ansatz reduces Eqs. (6)–(8) to coupled ordinary differential equations that can be solved using standard techniques

$$-u\frac{\partial N}{\partial s} + \frac{\partial}{\partial s}(NV) = 0, \tag{13}$$

$$-u\frac{\partial V}{\partial s} + V\frac{\partial V}{\partial s} = -\frac{\partial \Phi}{\partial s}, \tag{14}$$

$$\frac{\partial^2\Phi}{\partial s^2} - k_\perp^2\Phi = 1 - N. \tag{15}$$

In method 1, we directly integrate the equations. In method 2, we solve them via Fourier methods.

A. Method 1: Direct integration

In this method, it is useful to scale Eqs. (13)–(15) one more time, so as to remove the dependence on the parameter $k_\perp$. Define $\bar{u} = u\not{k}_\perp, \bar{v} = V\not{k}_\perp, \bar{s} = k_\perp s$, and $\bar{\Phi} = k_\perp^2\Phi$. Then, in these rescaled variables, Eqs. (13)–(15) become

$$-\bar{u}\frac{\partial N}{\partial \bar{s}} + \frac{\partial}{\partial \bar{s}}(N\bar{v}) = 0, \tag{16}$$

$$-\bar{u}\frac{\partial \bar{v}}{\partial \bar{s}} + \bar{v}\frac{\partial \bar{v}}{\partial \bar{s}} = -\frac{\partial \bar{\Phi}}{\partial \bar{s}}, \tag{17}$$

$$\frac{\partial^2\bar{\Phi}}{\partial \bar{s}^2} - \bar{\Phi} = 1 - N. \tag{18}$$

[Effectively, this rescaling replaces the factor k_1 by $k_\perp$ in the original scalings discussed after Eq. (3).] Direct integration of Eq. (16) then implies that

$$N(\bar{s}) = \Gamma/[\bar{u} - \bar{v}(\bar{s})], \tag{19}$$

where Γ is a constant of integration, related to the particle flux as seen in the moving frame. Equation (19) implies that $\bar{v}(s) < \bar{u}$ is necessary, otherwise there is a stagnation point where the density approaches infinity. Integration of Eq. (17) implies an energy conservation relation

$$\frac{1}{2}(\bar{u} - \bar{v}(\bar{s}))^2 + \bar{\Phi}(\bar{s}) = E, \tag{20}$$

which implies

$$\bar{u} - \bar{v}(s) = \sqrt{2(E - \bar{\Phi}(s))}. \tag{21}$$

In order to avoid singularities, Eq. (21) implies that

$$\bar{\Phi}(\bar{s}) \le E, \tag{22}$$

is required. Application of Eqs. (21) and (19) to Eq. (18) then yields

$$\frac{\partial^2\bar{\Phi}}{\partial \bar{s}^2} = -\frac{\partial \mathscr{V}}{\partial \bar{\Phi}}, \tag{23}$$

where the potential function $\mathscr{V}(\bar{\Phi})$ is

$$\mathscr{V}(\bar{\Phi}) = -\bar{\Phi} - \frac{1}{2}\bar{\Phi}^2 - \Gamma\sqrt{2(E - \bar{\Phi})}. \tag{24}$$

There are a range of Γ and E values for which $\mathscr{V}(\bar{\Phi})$ forms a potential well in which oscillatory solutions for $\bar{\Phi}(\bar{s})$ can be obtained from Eq. (23). A typical case is displayed in Fig. 1. There is a local minimum at $\bar{\Phi}_b$ and a local maximum at $\bar{\Phi}_a$.

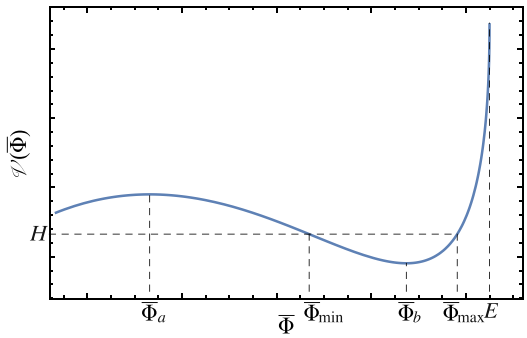

FIG. 1. The potential function $\mathscr{V}(\bar{\Phi})$.

Oscillations in $\bar{\Phi}$ occur between a minimum amplitude $\bar{\Phi}_{\min}$ and a maximum amplitude $\bar{\Phi}_{\max}$, with $\bar{\Phi}_a \le \bar{\Phi}_{\min} \le \bar{\Phi}_b$ and $\bar{\Phi}_{\max} \le E$ required.

The range of possible values of Γ and E for which oscillatory solutions occur is shown in Fig. 2. The upper limit on Γ is given by the curve $\Gamma = \sqrt{2E}$. On this curve, one of the two local extrema in V occurs at $\bar{\Phi} = 0$. When $E < 1/2$, this extremum is a local minimum, allowing small oscillations of $\bar{\Phi}$ around zero (i.e., linear waves). On the other hand, when $E > 1/2$ the extremum is a local maximum producing a soliton solution as discussed below. That is, solitons occur for $1/2 \le E \le 2$ and $\Gamma = \sqrt{2E}$, and linear waves occur along the same curve $\Gamma = \sqrt{2E}$ but with $0 \le E < 1/2$. Linear waves and solitons are analyzed in more detail below.

The minimum limit on possible Γ values for given E shown in Fig. 2 corresponds to waves with the maximum possible amplitude, $\bar{\Phi}_{\max} = E$ (see Eq. (22)). At this amplitude, there are stagnation points in the fluid where the density approaches infinity. The minimum and maximum curves meet at $\Gamma = E = 2$, which corresponds to a soliton with a stagnation point. The curves also meet at $\Gamma = E = 0$, where solutions become singular with wave numbers approaching infinity and amplitudes approaching zero; depending on how the limits $\Gamma \to 0$ and $E \to 0$ are taken the waves range from linear to highly nonlinear.

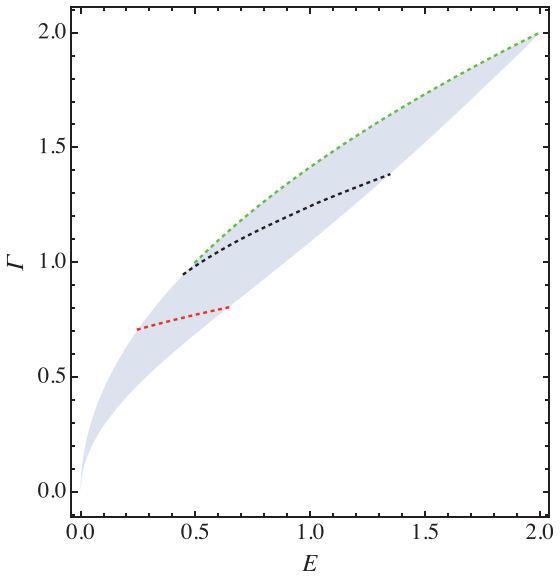

FIG. 2. The shaded area is the region in the E versus Γ plane for which nonlinear traveling-wave solutions occur. The red, black, and green dotted curves are contours of constant wavenumber $\bar{k}$ with values 1, 1/3, and zero, respectively. The zero-wavenumber solutions are solitons. Along each contour, the amplitude increases as one moves from left to right, from linear waves on the left to waves with stagnation points on the right.

From the form of the equation of motion, Eq. (23), there is an energy invariant H associated with the oscillation, given by

$$H = \frac{1}{2}\left(\frac{d\bar{\Phi}}{d\bar{s}}\right)^2 + \mathscr{V}(\bar{\Phi}), \tag{25}$$

where $H = \mathscr{V}(\bar{\Phi}_{\min}) = \mathscr{V}(\bar{\Phi}_{\max})$ (see Fig. 1). Note that H and $\bar{\Phi}_{\min}$ are both determined by $\bar{\Phi}_{\max}$. We will therefore parameterize our nonlinear solutions by $\bar{\Phi}_{\max}$, the maximum value of the potential during the oscillation.

These oscillatory solutions must satisfy certain constraints. Let us denote the wavelength of the oscillation as $\bar{\lambda}$ [i.e., the oscillatory solution obeys $\bar{\Phi}(\bar{s}+\bar{\lambda}) = \bar{\Phi}(\bar{s})$] and define an average over a period of oscillation as $\langle\rangle = \frac{1}{\bar{\lambda}}\int_{\bar{s}}^{\bar{s}+\bar{\lambda}} d\bar{s}$. Then, we require the solutions to obey the constraint

$$\langle N \rangle = 1, \tag{26}$$

i.e., mean density is unchanged from the equilibrium value. Taking an average of Eq. (20), using Eq. (26) and the identity $\langle d^2\bar{\Phi}/d\bar{s}^2\rangle = 0$ then implies that our solutions must obey

$$\langle \bar{\Phi} \rangle = 0. \tag{27}$$

In addition to these constraints, we require that the mean flow velocity vanishes

$$\langle N\bar{v} \rangle = 0. \tag{28}$$

This equation defines the lab frame of reference. In other words, the velocity of the wave, $\bar{u}$, is measured with respect to the frame in which the mean fluid velocity vanishes. In this frame, fluid elements oscillate in the wave but there is no net translation of the fluid.

An expression for the phase velocity can then be found by multiplying both sides of Eq. (19) by $\bar{u} - \bar{v}$ and taking the mean

$$\langle N\bar{u} \rangle - \langle N\bar{v} \rangle = \bar{u} = \Gamma, \tag{29}$$

where on the left hand side we applied Eqs. (26) and (28).

Now, Eq. (25) can be used to obtain an expression for the wavelength $\bar{\lambda}$. This equation implies that

$$d\bar{s} = d\bar{\Phi}/\sqrt{2[H - \mathscr{V}(\bar{\Phi})]}. \tag{30}$$

Integrating both sides over a half-period of the oscillation, during which $\bar{\Phi}$ varies from $\bar{\Phi}_{\min}$ to $\bar{\Phi}_{\max}$, implies that

$$\bar{\lambda} = 2\int_{\bar{\Phi}_{\min}}^{\bar{\Phi}_{\max}} \frac{d\bar{\Phi}}{\sqrt{2\left(\mathscr{V}(\bar{\Phi}_{\max}) - \mathscr{V}(\bar{\Phi})\right)}}, \tag{31}$$

where we have used $H = \mathscr{V}(\bar{\Phi}_{\max})$. This shows that $\bar{\lambda} = \bar{\lambda}(E, \Gamma, \bar{\Phi}_{\max})$. (The dependences on Γ and E arise through the dependence of V on these variables; see Eq. (24); and we again note that $\bar{\Phi}_{\min}$ depends on $\bar{\Phi}_{\max}$ through the relation $\mathscr{V}(\bar{\Phi}_{\min}) = \mathscr{V}(\bar{\Phi}_{\max})$.) However, Eq. (27) implies a relation between Γ, E, and $\bar{\Phi}_{\max}$

$$\int_0^{\bar{\lambda}} d\bar{s}\, \bar{\Phi}(\bar{s}) = 0.$$

Assuming that $\bar{s} = 0$ corresponds to $\bar{\Phi} = \bar{\Phi}_{\max}$, we convert the integration over $\bar{s}$ to one over $\bar{\Phi}$ using Eq. (30), to obtain

$$\int_{\bar{\Phi}_{\min}}^{\bar{\Phi}_{\max}} \frac{d\bar{\Phi}\, \bar{\Phi}}{\sqrt{2\left(\mathscr{V}(\bar{\Phi}_{\max}) - \mathscr{V}(\bar{\Phi})\right)}} = 0. \tag{32}$$

For given values of E and $\bar{\Phi}_{\max}$, Eq. (32) can be solved for Γ to obtain $\Gamma = \Gamma(E, \bar{\Phi}_{\max})$. This, together with Eq. (31), allows us to determine the wavelength $\bar{\lambda}$ as a function of E and $\bar{\Phi}_{\max}$. Thus, for given mode amplitude $\bar{\Phi}_{\max}$, the wavelength may be varied by changing E. In Fig. 3, we plot the range of possible wave numbers $\bar{k}(E, \bar{\Phi}_{\max}) = 2\pi/\bar{\lambda}(E, \bar{\Phi}_{\max})$ for given amplitude $\bar{\Phi}_{\max}$. There is a maximum possible wavenumber for a given mode amplitude $\bar{\Phi}_{\max}$, corresponding to the case where $E = \bar{\Phi}_{\max}$, which results in the aforementioned stagnation points where $\bar{v}(\bar{s}) = \bar{u}$ and $N(\bar{s}) \to \infty$ at the values of $\bar{s}$ where $\bar{\Phi} = \bar{\Phi}_{max} = E$. The figure shows that for infinitesimal amplitude (linear waves) all wave numbers are allowed, but as $\bar{\Phi}_{\max}$ approaches the maximum possible value of 2, the only allowed wavenumber is zero (i.e., a soliton with a stagnation point). Soliton solutions with lower amplitudes correspond to $\bar{k} = 0$ in this figure. For the periodic boundary conditions of interest in this paper, only certain discrete values of $\bar{k}$ are allowed, given by $\bar{k} = m/k_\perp$ for integer m.

Finally, the nonlinear wave phase velocity follows from the wave speed equation (29):

$$\bar{u}(E, \bar{\Phi}_{\max}) = \Gamma(E, \bar{\Phi}_{\max}). \tag{33}$$

We can invert $\bar{k} = \bar{k}(E, \bar{\Phi}_{\max})$ to obtain $E = E(\bar{k}, \bar{\Phi}_{\max})$ and use this to write $\bar{u} = \Gamma(E(\bar{k}, \bar{\Phi}_{\max}), \bar{\Phi}_{\max})$, i.e., wave phase velocity versus wavenumber and amplitude. This is plotted in Fig. 4 for four different amplitudes. The dashed line is for amplitude approaching zero

$$\bar{u}(\bar{k}, \bar{\Phi}_{\max} = 0) = 1/\sqrt{1 + \bar{k}^2}, \tag{34}$$

which corresponds to the phase velocity given by the linear dispersion relation (12) in barred units where $\bar{k} = m/k_\perp$ and $\bar{u} = k_\perp u$.

Fig. 5 displays the potential, density, and velocity versus position $\bar{s}$ for waves with $\bar{k} = 1/3$ and for several different amplitudes, and Fig. 6 displays the potential for waves with $\bar{k} = 0$ (i.e., solitons). The potential was determined by first finding the values of E and Γ corresponding to $\bar{k} = 1/3$ and the given values of $\bar{\Phi}_{\max}$, and then solving Eq. (23) numerically for these values. For small amplitude, the waves are nearly sinusoidal, but as the amplitude grows the waves become more sharply peaked until at the maximum possible amplitude the stagnation point produces a cusp in the potential and velocity functions, and a singularity in the density. Comparing Figs. 5 and 6, one can see that at larger amplitudes the soliton solutions are qualitatively similar to the finite $\bar{k}$ solutions.

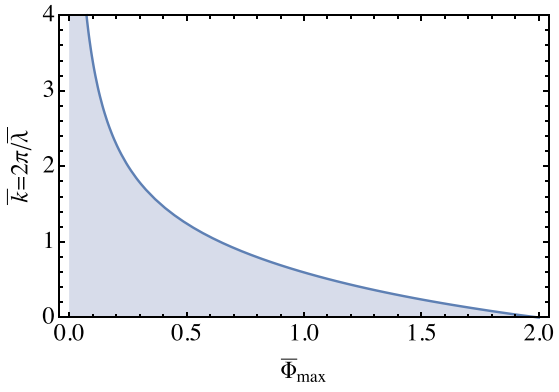

FIG. 3. The shaded area gives the region of allowed wavenumber $\bar{k}$ versus mode amplitude $\bar{\Phi}_{\max}$.

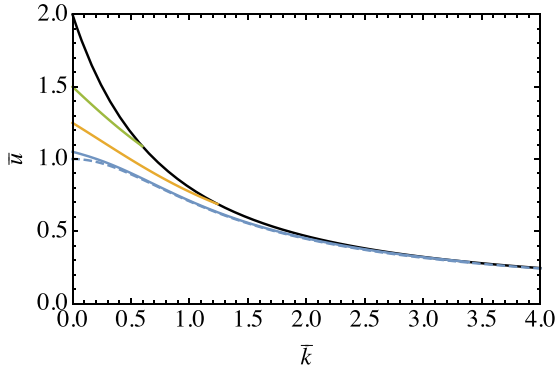

FIG. 4. The phase velocity $\bar{u}$ of traveling waves versus wavenumber $\bar{k}$ for four different amplitudes, $\bar{\Phi}_{\max} = 0$ (the dashed line), as well as $\bar{\Phi}_{\max} = 0.1, 0.5$, and 1, in order of increasing magnitude of $\bar{u}$ in the plot. The solid black line is the outer envelope of allowed velocities and wavenumbers.

1. Linear waves and solitons

Small amplitude waves can be analyzed by Taylor-expansion of the potential function $\mathbf{V}(\bar{\Phi})$, Eq. (24), in small $\bar{\Phi}$

$$\mathscr{V}(\bar{\Phi}) \simeq -\sqrt{2E}\Gamma + \left(\frac{\Gamma}{\sqrt{2E}} - 1\right)\bar{\Phi} + \frac{1}{2}\left(\frac{\Gamma}{(2E)^{3/2}} - 1\right)\bar{\Phi}^2 + \frac{\Gamma}{2(2E)^{5/2}}\bar{\Phi}^3 + \cdots \tag{35}$$

For linear waves, it is sufficient to keep only up to the quadratic terms in $\bar{\Phi}$, which provide a harmonic well for the potential oscillations. Such oscillations must satisfy Eq. (27), and therefore the coefficient of the linear term in $\bar{\Phi}$ in Eq. (35) must vanish, which implies $\Gamma = \sqrt{2E}$ for linear waves.

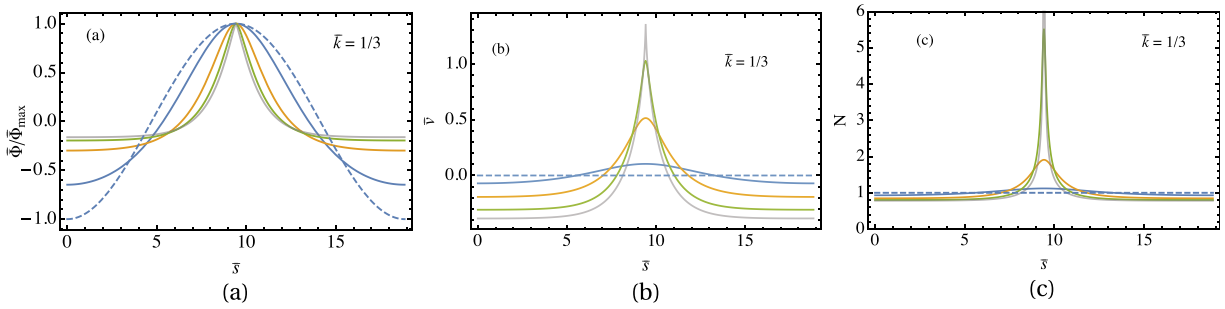

FIG. 5. Plots of the wave potential (a), fluid velocity (b), and density (c) for traveling waves over one wavelength $\bar{\lambda}$, all with $\bar{k} = 1/3$ (i.e., $\bar{\lambda} = 6\pi$), and with 5 different wave amplitudes: $\bar{\Phi}_{max} \to 0$ (the dashed line), and in order of increasing narrowness, $\bar{\Phi}_{max} = 0.1, 0.5, 1$, and the maximum possible value at $\bar{k} = 1/3$, $\bar{\Phi}_{max} = 1.34$ (see Fig. 3).

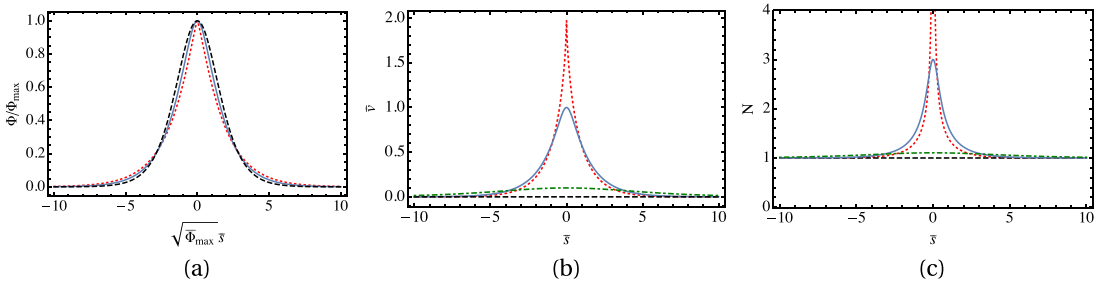

FIG. 6. (a) Wave potential versus position in solitons for three amplitudes: $\bar{\Phi}_{max} \to 0$, (dashed), $\bar{\Phi}_{max} = 1$, (solid), and $\bar{\Phi}_{max} = 2$ (dotted). The potential is scaled to $\bar{\Phi}_{max}$ and distance is scaled by $\sqrt{\bar{\Phi}_{max}}$ so that the infinitesimal amplitude soliton, Eq. (40), is visible in the plot. (b) and (c) Fluid velocity and density versus position in solitons, for the same amplitudes as in (a) as well as amplitude $\bar{\Phi}_{max} = 0.1$ (the dotted-dashed curve).

When this relation is employed in Eq. (35), the coefficient of the quadratic term in $\bar{\Phi}$ provides the frequency (actually, the wavenumber $\bar{k}$ since $\bar{s}$ is a position) of harmonic oscillations in the potential

$$\bar{k}^2 = \left(\frac{1}{2E} - 1\right). \tag{36}$$

Since the square of the wavenumber should be positive-definite for oscillatory solutions, this implies that $E < 1/2$ is required for linear waves, as discussed previously in relation to Fig. 2. The linear dispersion relation then follows from Eq. (29), which implies $\bar{u} = \sqrt{2E}$. Applying this relation to Eq. (36) yields $\bar{k}^2 = 1/\bar{u}^2 - 1$, which can be rearranged to produce the linear dispersion relation, Eq. (34).

Solitons occur when $\bar{\Phi}_{min}$ coincides with the local maximum $\bar{\Phi}_a$, so that the period of oscillation in the potential well $\mathscr{V}(\bar{\Phi})$ approaches infinity (see Fig. 1). However, the requirement that $\langle\bar{\Phi}\rangle = 0$ then implies that $\bar{\Phi}_{min} = \bar{\Phi}_a = 0$. From Eq. (35), the local maximum $\bar{\Phi}_a$ equals zero when $\Gamma = \sqrt{2E}$ and $E > 1/2$. This is the dotted green curve in Fig. 2.

The soliton amplitude $\bar{\Phi}_{max}$ is related to E by the potential function $\mathscr{V}(\bar{\Phi})$. Since $\mathscr{V}(\bar{\Phi}_{max}) = \mathscr{V}(\bar{\Phi}_{min})$, using Eq. (24) for $\mathscr{V}(\bar{\Phi})$, $\Gamma = \sqrt{2E}$, and $\bar{\Phi}_{min} = 0$ then implies

$$-\bar{\Phi}_{max} - \frac{1}{2}\bar{\Phi}_{max}^2 - 2E\sqrt{1 - \bar{\Phi}_{max}/E} = -2E. \tag{37}$$

This equation can be solved for $\bar{\Phi}_{max}$, yielding

$$\bar{\Phi}_{max} = 2(\sqrt{2E} - 1). \tag{38}$$

Since the soliton amplitude must satisfy Eq. (22), when combined with Eq. (38) this implies $1/2 \le E \le 2$ for soliton solutions, as shown in Fig. 2.

The soliton velocity versus amplitude follows from Eqs. (29), (38), and the relation $\Gamma = \sqrt{2E}$. From Eq. (29), this last relation implies $\bar{u} = \sqrt{2E}$. Combining this with Eq. (38) and rearranging yields

$$\bar{u} = 1 + \frac{1}{2}\bar{\Phi}_{max}. \tag{39}$$

Thus, the maximum possible soliton velocity $\bar{u} = 2$ occurs at the maximum amplitude $\bar{\Phi}_{max} = 2$, as shown in Fig. 4. Also, the maximum fluid velocity in the frame of the soliton is $\bar{v}(0) = \bar{\Phi}_{max}$. This follows from Eqs. (21), (38), and (39).

The functional form of solitons, $\bar{\Phi}(\bar{s})$, can be found by integrating both sides of Eq. (30) to obtain $\bar{s}(\bar{\Phi})$, and then inverting this expression. In general, the solitons can be expressed in terms of elliptic integrals but the form is too complex to merit reproduction here. Alternatively, they can be found by numerically integrating the equation of motion, Eq. (23). Solitons are shown in Fig. 6 for a range of amplitudes. The functional form simplifies in two cases. For small amplitudes, the solitons become K-dV solitons with functional form

$$\bar{\Phi}(\bar{s}) = \frac{\bar{\Phi}_{max}}{\cosh^2\left(\bar{s}\sqrt{\bar{\Phi}_{max}}/2\right)}. \tag{40}$$

For the maximum amplitude $\bar{\Phi}_{max} = 2$, the soliton has a stagnation point and can be expressed as the solution to the following equation:

$$-|\bar{s}| = -2\ln\left[2 - y - \sqrt{(1-y)(3-y)}\right] + \frac{2}{\sqrt{3}}\ln\left[\frac{3-2y-\sqrt{3(1-y)(3-y)}}{y}\right], \quad (41)$$

where $\bar{\Phi} = 2y(\frac{2}{3} - y)$.

B. Method 2: Fourier expansion

In this subsection, we apply Fourier methods to determine the same nonlinear traveling-wave solutions as were discussed in Sec. III A. The Fourier expansion method has several advantages. First, the periodic boundary conditions used in this paper are built directly into the method: the wavenumber k discussed in Sec. III A is no-longer a continuous variable but instead is automatically quantized to the correct values for a given plasma length. Second, we will see later that the method can also be applied to nonlinear standing wave solutions. Third, the Fourier method can be extended in a natural way to allow determination of the stability of traveling and standing wave solutions. Finally, some analytic results for low amplitude traveling waves can be readily obtained using Fourier expansion, because at low amplitudes the waves approach single Fourier modes.

In the Fourier approach, the traveling wave is expanded as a sum of spatial Fourier modes, each with fundamental period L. In the scaled units of Sec. III A, this period is 2π, and the Fourier expansions take the following form:

$$N(s) = \sum_{m=-\infty}^{\infty} N_m e^{ims}, \quad (42)$$

$$V(s) = \sum_{m=-\infty}^{\infty} V_m e^{ims}, \quad (43)$$

$$\Phi(s) = \sum_{m=-\infty}^{\infty} \Phi_m e^{ims}. \quad (44)$$

Also, Eqs. (26) and (28) imply that the $m=0$ Fourier coefficients must satisfy $N_0 = 1$ and $\Phi_0 = 0$.

In this section, we choose to work in a moving frame, one where $\langle V\rangle = 0$, rather than the frame implied by Eq. (27). In this new frame, we call the phase velocity u'. It differs from u by the value of $\langle NV\rangle$ as seen in the new frame

$$u = u' - \langle NV\rangle = u' - \sum_{m=-\infty}^{\infty} N_m V_{-m}. \quad (45)$$

We make this frame change because the condition $\langle V\rangle = 0$ is simple to implement in the Fourier method, requiring only that we set Fourier mode $V_0 = 0$. Once we have obtained the solution in the moving frame, we can use Eq. (45) to determine u in the lab frame.

First, we use Eqs. (42) and (44) in Eq. (8) to obtain the following relation between density and potential:

$$\Phi_m = \frac{N_m}{m^2 + k_\perp^2}. \quad (46)$$

Next, substituting these expansions into Eqs. (6) and (7) and taking the mth Fourier harmonic ($m \neq 0$) of the resulting equations imply

$$-u' m N_m + m\sum_{l=-\infty}^{\infty} V_l N_{m-l} = 0, \quad (47)$$

$$-u' m V_m + \sum_{l=-\infty}^{\infty} l V_l V_{m-l} = -\alpha_m N_m, \quad (48)$$

where

$$\alpha_m \equiv m/(m^2 + k_\perp^2). \quad (49)$$

Equations (47) and (48) constitute a nonlinear eigenvalue problem for the $m \neq 0$ Fourier coefficients N_m and v_m, where the eigenvalue is the phase velocity u'. There is always a trivial solution to these equations, $N_m = v_m = 0$; but for special values of u' there are nontrivial solutions corresponding to nonlinear traveling waves.

Symmetry in these equations allows us to specify, without loss of generality, that all the Fourier coefficients are real and satisfy $N_{-m} = N_m$ and $v_{-m} = v_m$, so that the traveling-wave solutions are even in s. Thus, we need only consider the $m > 0$ Fourier coefficients as independent variables in the equations.

Due to spatial homogeneity of the system, any eigenmode with period 2π and a given value of the perpendicular wavenumber $k_\perp$ can be mapped, by rescaling distances, into an infinite set of other eigenmodes with period $2\pi/l$ for integer l greater than one, each eigenmode with perpendicular wavenumber $lk_\perp$, and wave velocity u'/l. Therefore, we consider only the lowest-order eigenmode with period 2π, over a range of $k_\perp$ values, and a range of amplitudes. For small amplitudes, this eigenmode is concentrated in the $m=1$ Fourier harmonic.

In order to find these nontrivial solutions, we first approximate the equations by keeping only a finite number of Fourier modes, allowing m to range only over $-M \le m \le M$ for integer $M > 0$, and setting all Fourier coefficients outside this range equal to zero. Equations (47) and (48) then involve $2M$ independent equations in the $2M$ independent unknowns N_m and v_m, $1 \le m \le M$ (the $m < 0$ equations and unknowns are not independent).

We next parametrize the wave amplitude by the first Fourier coefficient of the density, N_1, i.e., we set this coefficient equal to a given amplitude value A, a real number greater than or equal to zero. This removes one of the unknown variables from the set of equations and makes the equations inhomogeneous. However, noting that u' is also an unknown quantity, we can now solve the $2M$ inhomogeneous nonlinear equations for u' along with the $2M-1$ unknown Fourier coefficients. Since the equations are now inhomogeneous their solution is fairly straightforward, parametrized by the values of A and $k_\perp$. For small amplitudes, the solution can be obtained using perturbation theory, and for larger amplitudes we use Newton's method. The solutions match those found in Sec. III A provided that a sufficiently large value of M is used. This becomes problematic for waves

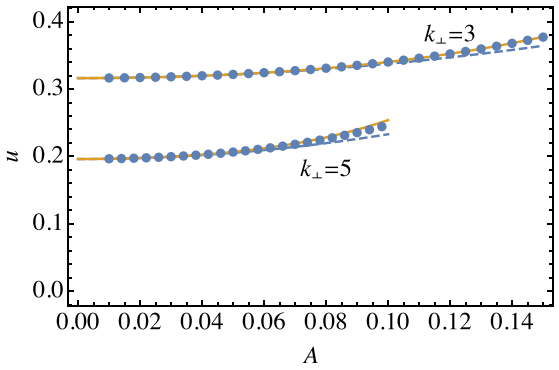

FIG. 7. The phase velocity u of traveling waves versus Fourier amplitude A for two transverse wave numbers, $k_\perp = 3$ and $k_\perp = 5$. Dots: numerical solution of Eqs. (47) and (48). Solid lines: Eq. (68). Dashed lines: the same expression, neglecting the A^4 term.

with stagnation points, where the density exhibits a singularity and its Fourier expansion converges slowly; or for solitons, which are not periodic; but for moderate amplitudes and finite wavelengths the Fourier method works well.

In Fig. 7, the wave phase velocity u is plotted versus amplitude A for two values of $k_\perp$. The phase velocity was obtained using the Fourier approach by numerically solving Eqs. (47) and (48) via Newtons method as described above, keeping $M = 40$ Fourier modes. Once u' was found from this solution, Eq. (45) was applied to determine u. The phase velocity is compared to perturbation expansions obtained below. As expected from Sec. III A, the phase velocity increases with increasing wave amplitude. Note that $k_\perp = 3$ and $k_\perp = 5$ correspond to $\bar{k} = 1/3$ and $\bar{k} = 1/5$, respectively, in Fig. 4. In Fig. 8, we plot the maximum wave potential $\Phi_{\max} = \Phi(s = 0)$ and maximum density $N_{\max} = N(s = 0)$ versus the Fourier amplitude coefficient A for different values of $k_\perp$. At low amplitudes, the maximum density is $N_{\max} = 1 + 2A$ and the maximum potential is $\Phi_{\max} = 2A/(1 + k_\perp^2)$. [In order to compare Figs. 7 and 8 to results in Sec. III A, recall that $\bar{\Phi} = k_\perp^2 \Phi$ and $\bar{u} = k_\perp u$.]

Figures 7 and 8 show that as $k_\perp$ increases, waves are more nonlinear for a given amplitude (i.e., they depart more from linear theory). This is because larger $k_\perp$ implies less linear dispersion, and it is dispersion that acts against the steepening effect of nonlinearity in these waves. Ultimately, in the limit of no dispersion (i.e., $k_\perp \to \infty$), even infinitesimal amplitude waves will exhibit nonlinear steepening and wave-breaking, in the absence of mitigating effects not included in our theory, such as viscosity.

1. Small amplitude perturbation expansion

For small amplitudes, $A \ll 1$, a perturbative solution of Eqs. (47) and (48) can be found by expanding the variables in powers of A. We assume that $N_m = 0(A^m)$ for $m > 1$, and similarly for v_m. In detail, we substitute the following perturbative expansions into Eqs. (46)–(48):

$$N_m = A^m \sum_{n=0}^{\infty} A^{2n} N_{m,2n}, m > 1, \tag{50}$$

$$V_m = A^m \sum_{n=0}^{\infty} A^{2n} v_{m,2n}, m > 0, \tag{51}$$

$$u' = \sum_{n=0}^{\infty} A^{2n} u_{2n}. \tag{52}$$

We then collect powers of A and solve the equations at each order of A in the unknown expansion coefficients appearing at that order, assuming that $N_1 = A$.

At first order in A, Eqs. (47) and (48) are nontrivial only for $m = 1$, becoming the linearized equations

$$-u_0 A + A v_{1,0} = 0, \tag{53}$$

$$-A u_0 v_{1,0} = -\alpha_1 A. \tag{54}$$

Solving Eqs. (53) and (54) for $v_{1,0}$ and u_0 yields the linear dispersion relation (see Eq. (34) for $m = 1$) as well as the linear fluid velocity coefficient

$$u_0^2 = \alpha_1, \tag{55}$$

$$v_{1,0} = u_0. \tag{56}$$

At second order in A, nontrivial terms appear only in the $m = 2$ equations, which become, after using Eqs. (55) and (56)

$$2(-u_0 N_{2,0} + v_{2,0} + u_0) = 0, \tag{57}$$

$$\alpha_2 N_{2,0} - 2u_0 v_{2,0} + \alpha_1 = 0. \tag{58}$$

When solved for $N_{2,0}$ and $v_{2,0}$, these equations yield

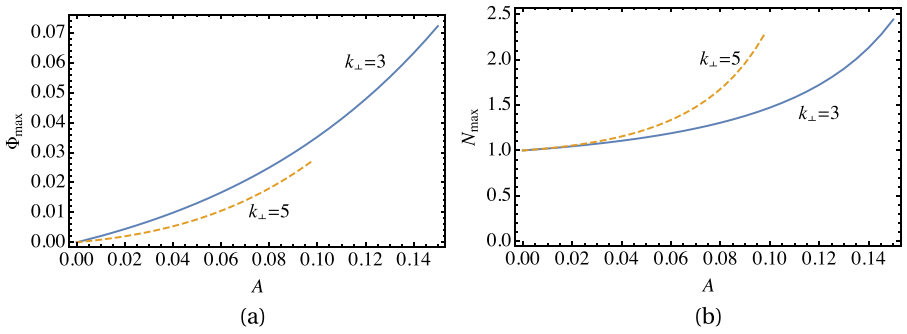

FIG. 8. (a) Maximum traveling-wave potential versus Fourier amplitude A for two transverse wave numbers. (b) Maximum density versus Fourier amplitude A for the same two transverse wave numbers.

$$N_{2,0} = \frac{3\alpha_1}{2\alpha_1 - \alpha_2}, \tag{59}$$

$$v_{2,0} = u_0 \frac{\alpha_1 + \alpha_2}{2\alpha_1 - \alpha_2}. \tag{60}$$

At third order in A, Eqs. (47) and (48) are nontrivial for $m = 1$ and $m = 3$. The $m = 1$ equations involve $v_{1,2}$ and u_2

$$(2\alpha_1 - \alpha_2)(v_{1,2} - u_2) + u_0(4\alpha_1 + \alpha_2) = 0, \tag{61}$$

$$(2\alpha_1 - \alpha_2)(v_{1,2} + u_2) - u_0(\alpha_1 + \alpha_2) = 0. \tag{62}$$

Solution of these equations yields the lowest-order nonlinear correction to the wave phase velocity

$$u_2 = u_0 \frac{5\alpha_1 + 2\alpha_2}{2(2\alpha_1 - \alpha_2)}, \tag{63}$$

as well as the fluid velocity Fourier coefficient

$$v_{1,2} = -u_0 \frac{3\alpha_1}{2(2\alpha_1 - \alpha_2)}. \tag{64}$$

Working to higher order, the next correction to the wave phase velocity is found to be

$$u_4 = \frac{3u_0}{8} \frac{18\alpha_1^4 + 9\alpha_1^2\alpha_2(12\alpha_2 - 5\alpha_3) + 4\alpha_2^3\alpha_3 + 12\alpha_1\alpha_2^2(3\alpha_2 + \alpha_3) - \alpha_1^3(45\alpha_2 + 206\alpha_3)}{(2\alpha_1 - \alpha_2)^3(3\alpha_1 - \alpha_3)}. \tag{65}$$

Using Eqs. (49), (63), and (65) in Eq. (52), the perturbation expansion for the wave phase velocity can be expressed as

$$u'/u_0 = 1 + \frac{A^2}{4}(8 + 3k_\perp^2) + \frac{A^4}{64}(128 + 208k_\perp^2 + 65k_\perp^4 + 3k_\perp^6) + 0(A^6). \tag{66}$$

However, u' is the phase velocity in a moving frame where $\langle V \rangle = 0$. In the lab frame where $\langle NV \rangle = 0$, the velocity u is related to u' by Eq. (45). In the moving frame, the value of $\langle NV \rangle$ can be found using the Fourier coefficients determined in the previous analysis (see Eq. (45)). To lowest order, $\langle NV \rangle = 2A^2 v_{1,0} = 2A^2 u_0$. To next order, we find that

$$\frac{\langle NV \rangle}{u_0} = 2A^2 + \frac{9A^4\alpha_1\alpha_2}{(2\alpha_1 - \alpha_2)^2} + 0(A^6) = 2A^2 + \frac{A^4}{2}(1 + k_\perp^2)(4 + k_\perp^2) + 0(A^6). \tag{67}$$

Subtracting Eq. (67) from Eq. (66) yields the wave phase velocity in the lab frame

$$u/u_0 = 1 + \frac{3A^2}{4}k_\perp^2 + \frac{3A^4}{64}k_\perp^2(16 + 11k_\perp^2 + k_\perp^4) + 0(A^6). \tag{68}$$

This expansion is compared to the numerical solution of Eqs (47), (48), and (45) in Fig. 7, showing good agreement for low to moderate wave amplitudes.

Note that as $k_\perp$ approaches zero, u approaches u_0, independent of wave amplitude. This is as expected from the general arguments given in Appendix A. Cold Langmuir waves with $k_\perp = 0$ have an amplitude-independent frequency, and therefore their phase velocity is also independent of amplitude.

IV. STANDING WAVE SOLUTIONS

We now obtain standing wave solutions to Eqs. (6)–(8). For a long, thin plasma column, it has been shown that standing TG waves satisfy approximate Neumann boundary conditions on the potential: $d\Phi/dz(z = 0) = d\Phi/dz(z = \pi) = 0$.[16] A Fourier expansion of the variables consistent with these boundary conditions is

$$N(z,t) = \sum_{m=0}^{\infty} N_m(t)\cos mz, \tag{69}$$

$$\Phi(z,t) = \sum_{m=1}^{\infty} \Phi_m(t)\cos mz, \tag{70}$$

$$V(z,t) = \sum_{m=1}^{\infty} V_m(t)\sin mz, \tag{71}$$

where $N_0(t) = 1$, and where Eq. (8) implies

$$\Phi_m(t) = \frac{N_m(t)}{m^2 + k_\perp^2}. \tag{72}$$

These expansions are substituted into Eq. (6), and the $\cos mz$ coefficient of the result is taken, yielding

$$\dot{N}_m(t) + \frac{m}{2}\sum_{m'=1}^{\infty} V_{m'}[N_{m-m'} + N_{m'-m} - N_{m+m'}] = 0. \tag{73}$$

Here, note that $N_m = 0$ for $m < 0$, which can be used to change the limits in the sum over m' for the first two terms in the square bracket. Also, note that the $m = 0$ version of Eq. (73) is trivially satisfied by $N_0 = 1$ and will therefore not be used in the following arguments.

Similarly, the $\sin mz$ coefficient of Eq. (7) is

$$\dot{V}_m(t) + \frac{1}{2}\sum_{m'=1}^{\infty} m' V_{m'}[V_{m-m'} - V_{m'-m} + V_{m+m'}] = \alpha_m N_m. \tag{74}$$

Here as well, note that $V_m(t) = 0$ for $m \le 0$.

We are concerned here with standing wave solutions that are periodic in time, so $N_m(t)$ and $V_m(t)$ each have subsidiary Fourier series expansions in time

$$N_m(t) = \sum_{n=0}^{\infty} N_{m,n} \cos n\omega t, \tag{75}$$

$$V_m(t) = \sum_{n=1}^{\infty} v_{m,n} \sin n\omega t, \tag{76}$$

where the frequency ω is an unknown variable. When these expansions are substituted into Eq. (73) and the $\sin n\omega t$ coefficient is taken, the result is

$$-n\omega N_{m,n} + \frac{m}{4}\sum_{m'=1}^{\infty}\sum_{n'=1}^{\infty} v_{m',n'}[N_{m-m',n-n'} + N_{m'-m,n-n'} - N_{m'+m,n-n'} + N_{m-m',n'-n} + N_{m'-m,n'-n} - N_{m'+m,n'-n} - N_{m-m',n'+n} + N_{m'-m,n'+n} - N_{m'+m,n'+n}] = 0. \tag{77}$$

Similarly, when the $\cos n\omega t$ coefficient of Eq. (74) is taken, the result is

$$n\omega v_{m,n} + \frac{1}{4}\sum_{m'=1}^{\infty}\sum_{n'=1}^{\infty} m' v_{m',n'}[-v_{m-m',n-n'} + v_{m'-m,n-n'} - v_{m'+m,n-n'} + v_{m-m',n'-n} - v_{m'-m,n'-n} + v_{m'+m,n'-n} + (v_{m-m',n'+n} - v_{m'-m,n'+n} + v_{m'+m,n'+n})(1-\delta_{n,0})] = \alpha_m N_{m,n}, \tag{78}$$

where $\delta_{n,0}$ is a Kronecker delta function. Equation (77) is valid for $m \geq 1$ and $n \geq 1$, while Eq. (78) is valid for $m \geq 1$ and $n \geq 0$.

Equations (77) and (78) are a nonlinear eigenvalue problem for standing waves, similar to Eqs. (47) and (48) for traveling waves. The equations can be solved using the same method as for Eqs. (47) and (48). First, the system is made finite by imposing a maximum wavenumber and frequency. We take $m \leq M$ and $n \leq M$, and set the Fourier coefficients $N_{m,n}$ and $v_{m,n}$ to zero beyond these ranges. Next, we take $N_{1,1} = A$ where A is a given real number greater than zero, the amplitude of the nonlinear wave. This picks out the eigenfunction with the lowest fundamental wavenumber, $m = 1$. (If instead we had taken $N_{1,1} = 0$ and $N_{2,1} = A$, we would have picked out an eigenfunction with fundamental wavenumber $m = 2$.) We then solve the equations for the other Fourier coefficients along with the mode frequency ω. The solution can be found either numerically via Newton's method or as a perturbation expansion in A, as was done for traveling waves. A symmetry of the equations implies that if m is even then only even n terms are nonzero, and if m is odd, only odd n terms are nonzero. This reduces the number of variables and equations to $M^2 + M/2$ (assuming M is even). Nevertheless, this problem is more difficult than the traveling-wave problem where the number of unknowns and equations scaled linearly with M, because there was no time dependence in the traveling-wave solution when viewed in the wave frame.

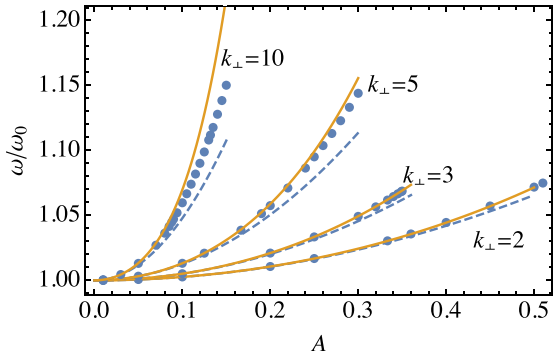

FIG. 9. Frequency versus amplitude A in nonlinear standing waves, normalized to the linear frequency ω_0, for four values of $k_\perp$. Points: frequency obtained from numerical solution of Eqs. (77) and (78). Dashed line: the lowest-order (A^2) correction to the frequency. Solid line: frequency including the A^4 correction. Both corrections are included in Eq. (101).

We have solved Eqs. (77) and (78) for a range of amplitudes A and for several $k_\perp$ values. In order to obtain converged solutions at the largest amplitudes, an M value of up to 60 was employed, requiring the numerical solution of 3630 coupled nonlinear equations using Newton's method. The frequency of the waves is displayed in Fig. 9 versus amplitude A for four values of $k_\perp$, and compared to perturbation expansions valid for small A, derived below. As amplitude increases, the wave frequency increases in a manner similar to the traveling wave case discussed previously.

The harmonic content of the waves increases as the amplitude of the wave increases. In Fig. 10, we display the Fourier coefficients N_{mm} versus amplitude, for $k_\perp = 5$. As A increases each coefficient increases roughly as $N_{m,m} \sim A^m$. This is the scaling expected in perturbation theory, as we will show in Sec. IV A.

The spatial form of the density is displayed in Fig. 11 at an instant of maximum amplitude, which occurs twice per period, for instance, at $t = 0$ and at $t = \pi/\omega$. At time $t = 0$, the density peak is at one end of the column, $z = 0$, and at $t = \pi/\omega$ the peak has shifted to the other end of the column, at $z = \pi$ ($z = L$ in unscaled units) (the instant shown in the figure, which displays $0 < z < 2L$ in unscaled units). At these times, the fluid velocity is zero. The spatial form at $t = \pi/\omega$ is identical to the form at $t = 0$, except for an overall

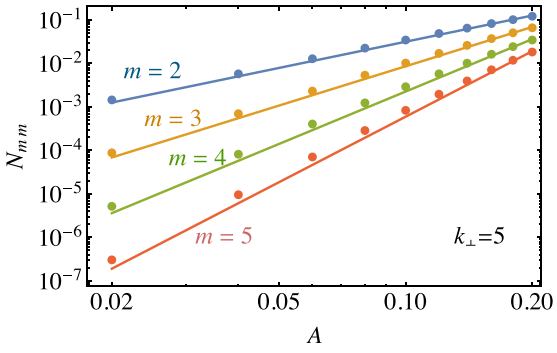

FIG. 10. Fourier coefficients $N_{m,m}$ in a nonlinear standing wave with $k_\perp = 5$, versus wave amplitude A. The lines are aids to the eye of the form A^m for $m = 2, 3, 4, 5$.

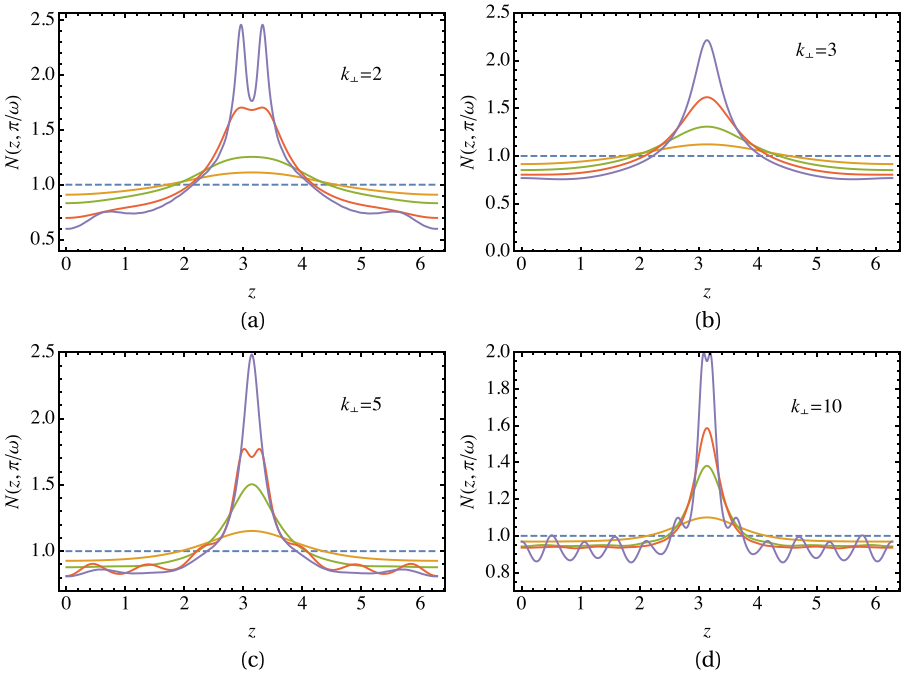

FIG. 11. Density versus position in nonlinear standing waves at an instant of maximum amplitude for four values of $k_\perp$, and for various amplitudes A. The dashed line is the equilibrium density. The amplitudes shown in (a) are $A = 0.1, 0.2, 0.4, 0.5$. In (b), the amplitudes are $A = 0.1, 0.2, 0.3, 0.4$. In (c), the amplitudes are $A = 0.1, 0.2, 0.25, 0.3$, and in (d), the amplitudes are $A = 0.05, 0.1, 0.12, 0.15$.

shift in position of the wave by π. At very low amplitudes, $A \ll 1$, the standing wave is nearly linear, consisting of two linear traveling waves moving in opposite directions, causing the density to "slosh" from one end of the column to the other, with stationary nodes. As the amplitude A of the fundamental Fourier mode increases, the standing wave density becomes more strongly peaked, and there are no-longer stationary nodes in the solution. The solution can then be crudely described as a soliton traveling from one end of the plasma column to the other, where it meets its counter-propagating periodic image and reflects from it (or passes through it).

The density is a smooth function of increasing amplitude A except at certain points where we observe jumps in the solution. One such point occurs for $k_\perp = 5$ in the range $A = 0.246 - 0.247$. The density for these two amplitudes is displayed in Fig. 12, and the peak density (i.e., the density at $z = 0$ and $t = 0$ or $z = \pi$ and $t = \pi/\omega$) is displayed versus A in Fig. 13. Near the jump, the density is rippled as shown in the figure, but these ripples are greatly reduced at slightly larger or smaller values of A. At the jump, the phase of the ripple changes abruptly. The behavior is similar to a resonance, in which a high order mode in the solution is excited by the fundamental. Across the jump, one solution disappears and is replaced by the other, i.e., solutions cannot be followed across the jump. For $k_\perp = 2$ and 3, we did not observe any jumps in the amplitude range, $0 < A < 0.5$, but this does not rule out that such jumps could occur for larger A values, or that the jumps were too small or narrow to observe. For $k_\perp = 10$, several observable jumps occur (see Fig. 13), with behavior similar to that shown in Fig. 12 in each case.

These jumps appear to be related to nonlinear degeneracies in the standing wave frequencies. A standing wave of frequency ω and amplitude A consists of multiple spatial and time Fourier harmonics. A given spatial Fourier harmonic m with frequency $n\omega$ may be resonant with a second standing wave with fundamental wavelength m and frequency $n\omega$. In

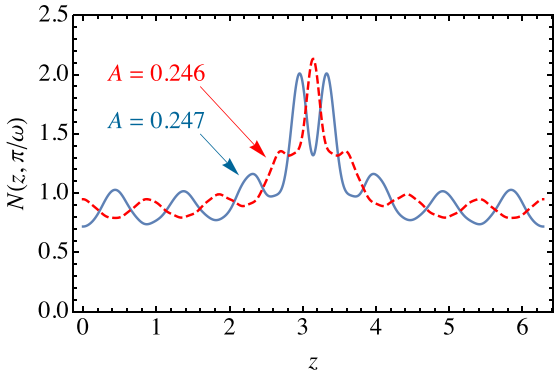

FIG. 12. Density versus position at an instant of maximum amplitude for $k_\perp = 5$ and for two close values of A, showing an apparent discontinuity in the behavior of the solution as a function of amplitude.

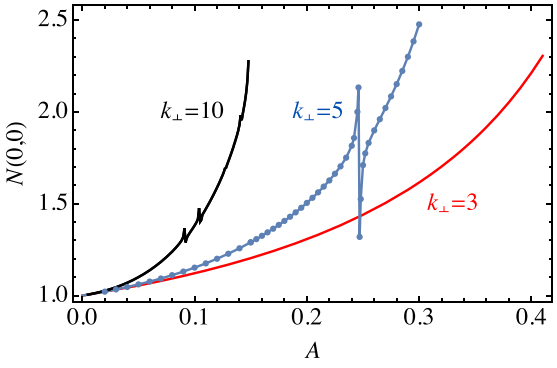

FIG. 13. Peak density (at $z = 0$ and $t = 0$) versus amplitude A for three values of $k_\perp$.

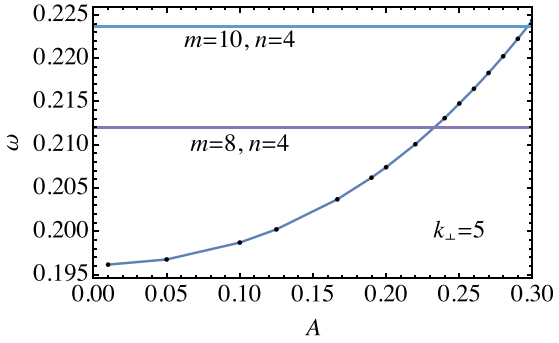

FIG. 14. Nonlinear degeneracies are plotted between a standing wave of frequency ω for $k_\perp = 5$ (curve), and linear embedded waves with wavenumber m and frequency $n\omega$. The horizontal lines are the linear frequencies ω_m, divided by n, for the only two m and n pairs that give degeneracy in the plotted range of amplitudes.

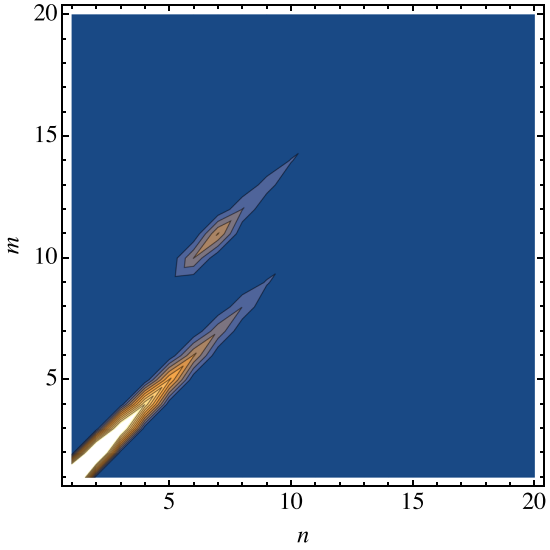

FIG. 15. Contour plot of the magnitude of the Fourier harmonics in the density, $N_{m,n}$, for a standing wave with frequency $\omega = 0.10599$, $k_\perp = 10$, and amplitude $A = 0.104$. This amplitude corresponds to the second jump in the $k_\perp = 10$ curve displayed in Fig. 13. The peak in the contour plot at $m = 11, n = 7$ corresponds to a near-degeneracy of the standing wave with a linear wave of frequency 7ω and wavenumber $m = 11$. This peak is only present near the given amplitude $A = 0.104$.

some sense, this second wave is embedded in the original standing wave and can be driven by it.

The amplitude at which these resonances occur can be predicted by assuming the embedded wave is of small amplitude, and comparing the linear frequency of such a wave, of wavenumber m, with a multiple n of the frequency of the standing wave, noting that if m is even then so is n, and if m is odd then so is n (as explained in the paragraph after Eq. (78)). Thus, we look for solutions of the equation

$$n\omega(A) = \omega_m, \tag{79}$$

where $\omega(A)$ is the standing wave frequency for amplitude A, and ω_m is the linear wave frequency for wavenumber m, given by Eq. (12).

For the $k_\perp = 5$ case, we find that there are only two solutions of Eq. (79) in the observable amplitude range. A linear wave with $m = 8$ and $n = 4$ is degenerate with the observed nonlinear standing wave at amplitude $A \sim 0.233$, which is fairly close to the observed location of the resonance, $A = 0.246 - 0.247$ (see Fig. 14). Furthermore, by counting peaks in Fig. 12, one can see that the ripple has $m = 8$. There is a second possible degeneracy with a $m = 10$ wave at $A \sim 0.3$, but this is just at the edge of the range of A values we can probe.

For the $k_\perp = 10$ case, Fig. 13 shows two jumps in the data at $A \sim 0.91$ and $A \sim 0.1$. Comparing the frequency data for this $k_\perp$ value to the linear dispersion relation, one finds that there is a $m = 8, n = 6$ degeneracy at $A \sim 0.893$ and a $m = 11, n = 7$ degeneracy at $A \sim 0.102$, closely matching the amplitudes at the observed jumps. In fact, examination of the Fourier harmonics in the standing wave near these two A values shows peaks in the amplitude of the harmonics at just these values of m and n. The magnitude of the density harmonics $N_{m,n}$ for the case $A = 0.104$ is displayed in Fig. 15. Aside from the main peak along the $m = n$ line, a second peak appears centered at $m = 11, n = 7$. This peak is visible in the data only for A near $A \sim 0.104$.

This type of nonlinear resonance phenomenon is related to harmonic generation in high intensity nonlinear optics; see Sec. VI. Such resonances could also be a fairly common occurrence in other weakly dispersive nonlinear systems such as shallow water waves or acoustic resonators. The weaker the dispersion, the stronger the nonlinear frequency shift, and the greater the chance of a solution to Eq. (79) in the available range of amplitudes.

We have tested that these nonlinear standing waves are actual periodic solutions of the fluid equations by solving Eqs. (6)–(8) numerically, using as initial conditions the density and velocity taken from solutions of Eqs. (77) and (78). The solutions of Eqs. (6)–(8) with these initial conditions oscillate as expected, with the periodicity predicted by the eigenvalue problem. The Galerkin method used in solving Eqs. (6)–(8) is discussed in Appendix B. In Fig. 16, we display a few numerically determined Fourier amplitudes versus time over a wave period. The numerical solution kept $M = 30$ spatial Fourier harmonics. A given spatial harmonic m is, for smaller m, dominated by time harmonic $n = m$, but can have a complex waveform for larger m, particularly at larger amplitudes A. These waveforms agree with the theoretically determined time-dependence given by Eqs. (75) and (76), with frequency and Fourier amplitudes determined by solution of the eigenvalue problem.

We have also created nonlinear standing wave solutions by driving the system with external forcing. This is similar to what is done in experiments, where TG waves are driven to large amplitude by applying an oscillatory signal to a cylindrical electrode at one end of the plasma column. When the frequency of the signal is close to that of a normal mode, that mode can be driven to large amplitude. In simulations of this process using Eqs. (6)–(8), we add a time and space-dependent external potential to the right-hand side of Eq. (7). The spatial dependence is chosen to be a single Fourier

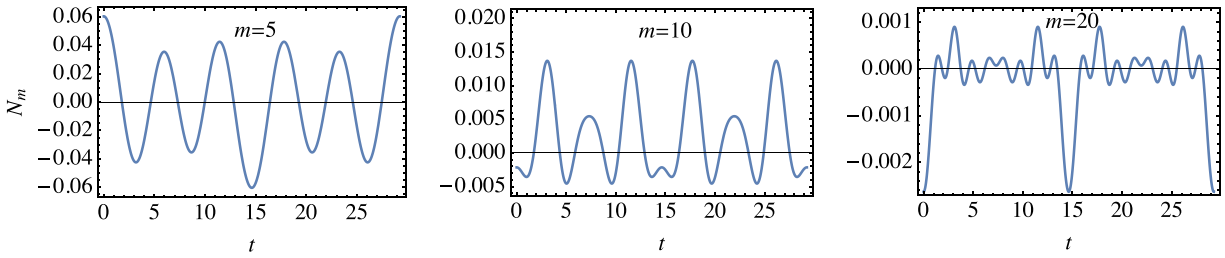

FIG. 16. Time dependence of three selected spatial Fourier harmonics, over one period of the standing wave, for $k_\perp = 5$ and $A = 0.25$.

cosine mode for the potential, and the time dependence is chosen to be a single frequency oscillation with a slowly varying Gaussian envelope. In order to excite large-amplitude standing waves, we find that the envelope of the forcing must be sufficiently slowly varying so that all of the harmonics in the wave have time to grow to the correct amplitude through nonlinear interactions with the forcing. We also find that it is useful to tune the frequency of the forcing to slightly above the natural frequency ω_0 of linear modes, to more closely match the nonlinear frequency of the standing waves we are trying to excite. Details of the forcing function used are discussed in Appendix B.

The Fourier method used in this section works for moderately large-amplitude standing waves, but breaks down if the wave amplitude is too large because too many Fourier modes must be kept for the method to practical. Consequently, several questions regarding very large amplitude standing waves cannot be considered using this method. For instance, is there a maximum amplitude for any given value of $k_\perp$, and if so, what is this amplitude and what happens to the wave as this amplitude is approached? For traveling waves, we have seen that stagnation points with infinite density form at the maximum amplitude. Does something like this happen for standing waves as well? For the analytically tractable case $k_\perp = 0$ discussed in Appendix A, such singularities were found to occur when characteristics of the fluid flow cross, and it is likely that something similar occurs for $k_\perp > 1$. At such points, the cold fluid equations break down, and new physics such as pressure effects must be added to regularize the equations.

A. Small amplitude perturbation expansion

In this subsection, we solve Eqs. (77) and (78) using a perturbation expansion, assuming the amplitude A is small. Just as for traveling waves, we assume that $N_m(t) = 0(A^m)$ and $v_m(t) = 0(A^m)$ (see Fig. 10). However, since the standing waves are time dependent as given explicitly by Eqs. (75) and (76), we also require ordering for the Fourier coefficients $N_{m,n}$ and $v_{m,n}$. We find that a consistent ordering is $N_{m,n} = 0(A^m)$ and $v_{m,n} = 0(A^m)$ for $n \le m$, and $N_{m,n} = 0(A^n)$ and $v_{m,n} = 0(A^n)$ for $n > m$. Recall also that if m is even(odd) then so is n, and that $N_{m,n}$ has nonzero $n = 0$ terms (for m even) while $v_{m,n}$ does not. Also, in general each coefficient, and the mode frequency, has a subsidiary expansion in A, taking the general form

$$N_{m,n} = A^{\max(m,n)} \sum_{o=0}^{\infty} A^{2o} N_{m,n,2o}, \tag{80}$$

$$v_{m,n} = A^{\max(m,n)} \sum_{o=0}^{\infty} A^{2o} v_{m,n,2o}, \tag{81}$$

$$\omega = \sum_{o=0}^{\infty} A^{2o} \omega_{2o}, \tag{82}$$

except for $N_{1,1}$, which is simply equal to the amplitude A. We substitute Eqs. (80)–(82), along with $N_{1,1} = A$, into Eqs. (77) and (78) and collect powers of A, solving the resulting equations order by order in A. To first order in A, only the $m = 1$ and $n = 1$ equations are nontrivial, yielding the linear equations

$$-\omega_0 A + A v_{1,1,0} = 0, \tag{83}$$

$$\omega_0 A v_{1,1,0} = \alpha_1 A, \tag{84}$$

which yield $v_{1,1,0} = \omega_0$ along with the linear dispersion relation

$$\omega_0^2 = \alpha_1. \tag{85}$$

At order A^2, the only nontrivial equations are the $m = 2, n = 2$ form of Eq. (77) and the $m = 2, n = 0$ and $n = 2$ forms of Eq. (78)

$$-2N_{2,2,0}\omega_0 + \frac{\omega_0}{2} + 2v_{2,2,0} = 0, \tag{86}$$

$$\frac{\alpha_1}{4} = N_{2,0,0}\alpha_2, \tag{87}$$

$$2\omega_0 v_{2,2,0} - \frac{\alpha_1}{4} = N_{2,2,0}\alpha_2. \tag{88}$$

The solution of these equations yields

$$N_{2,0,0} = \frac{\alpha_1}{4\alpha_2}, \tag{89}$$

$$N_{2,2,0} = \frac{3\alpha_1}{4(2\alpha_1 - \alpha_2)}, \tag{90}$$

$$v_{2,2,0} = -\omega_0 \frac{\alpha_1 + \alpha_2}{4(2\alpha_1 - \alpha_2)}. \tag{91}$$

At third order, there are nontrivial equations for both $m = 1$ and $m = 3$. The $m = 1$ equations are nontrivial for $n = 1$ and $n = 3$ and are

$$-\omega_2 - \omega_0 \frac{4\alpha_1^2 - 6\alpha_1\alpha_2 - \alpha_2^2}{16\alpha_2(2\alpha_1 - \alpha_2)} + \nu_{1,1,2} = 0, \tag{92}$$

$$-3\omega_0 N_{1,1,0} - \frac{\omega_0}{16} + \nu_{1,3,0} = 0, \tag{93}$$

$$\omega_0 \nu_{1,1,2} + \omega_0\omega_2 - \alpha_1 \frac{\alpha_1 + \alpha_2}{16(2\alpha_1 - \alpha_2)} = 0, \tag{94}$$

$$3\omega_0 \nu_{1,3,0} + \frac{\alpha_1(\alpha_1 + \alpha_2)}{16(2\alpha_1 - \alpha_2)} = \alpha_1 N_{1,3,0}. \tag{95}$$

The solution of these equations yields the Fourier coefficients

$$\nu_{1,1,2} = \omega_0 \frac{\alpha_1}{32\alpha_2} \frac{4\alpha_1 - 5\alpha_2}{2\alpha_1 - \alpha_2}, \tag{96}$$

$$N_{1,3,0} = \frac{2\alpha_2 - 7\alpha_1}{128(2\alpha_1 - \alpha_2)}, \tag{97}$$

$$\nu_{1,3,0} = -\omega_0 \frac{5\alpha_1 + 2\alpha_2}{128(2\alpha_1 - \alpha_2)}, \tag{98}$$

as well as the lowest-order nonlinear correction to the standing wave frequency

$$\omega_2 = \omega_0 \frac{2\alpha_2^2 + 7\alpha_1\alpha_2 - 4\alpha_1^2}{32\alpha_2(2\alpha_1 - \alpha_2)}. \tag{99}$$

Working to higher order, the next order correction to the frequency is found to be

$$\begin{aligned}\omega_4 = \omega_0[&960\alpha_1^7 - 180\alpha_2^5\alpha_3^2 + 12\alpha_1\alpha_2^4\alpha_3(-30\alpha_2 + 47\alpha_3) - 64\alpha_1^6(3\alpha_2 + 158\alpha_3) + \alpha_1^2\alpha_2^3(396\alpha_2^2 - 4952\alpha_2\alpha_3 - 2037\alpha_3^2)\\ &- 3\alpha_1^4\alpha_2(1591\alpha_2^2 + 7684\alpha_2\alpha_3 + 3136\alpha_3^2) + \alpha_1^5(-1350\alpha_2^2 + 28288\alpha_2\alpha_3 + 3264\alpha_3^2)\\ &+ 2\alpha_1^3\alpha_2^2(1434\alpha_2^2 + 5291\alpha_2\alpha_3 + 5517\alpha_3^2)]/[4096\alpha_2^2(2\alpha_1 - \alpha_2)^3(\alpha_1 - 3\alpha_3)(3\alpha_1 - \alpha_3)].\end{aligned} \tag{100}$$

Using Eqs. (82), (99), (100), and (49), the frequency of the nonlinear standing wave can be expressed as

$$\begin{aligned}\omega/\omega_0 = 1 &+ \frac{3A^2}{64}k_\perp^2 \frac{3 + k_\perp^2}{1 + k_\perp^2} + \frac{3A^4}{16384}k_\perp^2\\ &\times \frac{135 + 69k_\perp^2 + 74k_\perp^4 + 21k_\perp^6 + k_\perp^8}{\left(1 + k_\perp^2\right)^2} + 0(A^6).\end{aligned} \tag{101}$$

Note that all nonlinear corrections vanish as $k_\perp \to 0$. The frequency of a nonlinear cold plasma standing wave with $k_\perp = 0$ is independent of amplitude (in perturbation theory), as discussed in Appendix A and at the end of Sec. II.

Also note that the nonlinear frequency corrections for a standing wave are not the same as for a traveling wave, as given by Eq. (68). In linear theory, standing waves are merely a superposition of two counter-propagating traveling waves and have the same dispersion as traveling waves. But nonlinear standing waves obviously cannot be obtained as the sum of two nonlinear traveling waves, and consequently their dispersion differs.

In Fig. 9, we compare Eq. (101) to the frequencies found from numerical solution of Eqs. (77) and (78). We find good agreement provided that A and $k_\perp$ are sufficiently small. Just as for the case of traveling waves, as $k_\perp$ increases the waves have less dispersion to balance nonlinearity, waves of a given amplitude A are therefore more nonlinear, and perturbation expansions are less useful. Ultimately, for very large $k_\perp$, the TG waves are nearly dispersionless, and even small amplitude waves display large deviations from linear theory.

V. LINEAR STABILITY

In this section, we examine the linear stability properties of the nonlinear traveling and standing waves constructed in Secs. III–IV. We first present a simple and well-known 3-wave parametric resonance model of instability.[12–15] In this model, the nonlinear standing or traveling wave is described as a single Fourier mode with frequency ω_p and wavenumber p. (Such a model is correct only for nearly linear waves.) This "pump" wave interacts nonlinearly with two "daughter" waves, with frequencies ω_l and ω_m and wave numbers l and m, respectively. These waves are assumed to initially be of much smaller amplitude than the pump. The wave numbers must satisfy a momentum conservation relation $p = l + m$. Then when a resonance condition, $\omega_p = \omega_l + \omega_m$, is satisfied, one finds that the daughter waves grow exponentially in amplitude at the expense of the pump wave amplitude, since a beat mode between the pump wave and one of the daughter waves phase locks to the other daughter wave, allowing resonant energy exchange.

Furthermore, for finite pump amplitude, the resonance condition need not be perfectly satisfied, and yet this 3-wave system is still unstable. That is, define the linear detuning of the resonance as

$$\Delta\omega = \omega_l + \omega_m - \omega_p, \tag{102}$$

where the frequencies appearing in this expression are the small amplitude (linear) frequencies. Recall that there is a nonlinear shift of the pump wave frequency ω_p due to its finite amplitude, see Fig. 7 or 9. There are also nonlinear shifts of the daughter wave frequencies due to the pump. Consequently, the detuning is changed and can in fact be reduced to zero if the amplitude of the pump is sufficiently large, again allowing phase locking between the waves and resonant growth of the daughter waves at the expense of the pump wave.

However, the three-wave theory is at best a poor approximation when considering nonlinear TG waves. These waves, with $k_\perp > 1$, have fairly linear dispersion and are therefore strongly coupled to one-another by nonlinearity, as

we have seen in Secs. III–IV; hence, a three-wave model of the nonlinear system is inadequate. In order to test the validity of the three-wave model and to understand the actual linear stability properties of the TG waves, we use a Fourier representation of the perturbations on the nonlinear standing and traveling waves.

For traveling waves, in the wave frame, there is a time-independent equilibrium from which the system can be perturbed to obtain linear equations of motion for the perturbations. The eigenmodes of these equations are found, and growing modes are identified. However, for a given nonlinear wave amplitude A, we find that if the Fourier representation of the wave is sufficiently accurate, i.e., if the number of modes M kept in the representation is sufficiently large, none of the perturbing eigenmodes to the wave are unstable. We find this to be true for the full range of amplitudes we could study using the Fourier methods discussed in Sec. III B. This result is in strong contradiction to the three-wave model of parametric resonance. Furthermore, for smaller M values where instability is observed, the most unstable linear eigenmode bears little resemblance to either simple single mode daughter waves, or any nonlinear traveling wave or waves.

For nonlinear standing waves, the results of a linear stability analysis are rather different. Here, there is no time-independent equilibrium about which one can perturb. However, since the underlying wave is periodic in time a variant of Floquet analysis can be applied to determine the linear eigenmodes of the perturbations. We find that if the number of modes in the wave representation is sufficiently large, instability is suppressed but not eliminated. Over a range of amplitudes that depends on $k_\perp$, these eigenmodes are unstable. This range of amplitudes is in all cases far beyond that which is predicted by the three-wave model, and the growth rates are smaller than the three-wave prediction.

We have tested these results using fully nonlinear numerical solutions of the TG fluid equations (6)–(8) and have found good agreement with the eigenmode stability analysis. For the standing wave case, we find that a small seed added to a nonlinear standing wave can grow at the expected growth rate provided that the pump wave amplitude falls in the range predicted by the eigenmode analysis. For traveling waves, no growth is observed if the simulation keeps a sufficiently large number of modes.

A. Traveling waves

We now consider small perturbations to nonlinear traveling waves, writing

$$\begin{aligned} N(s,t) &= N(s) + \delta N(s,t), \\ V(s,t) &= V(s) + \delta V(s,t), \\ \Phi(s,t) &= \Phi(s) + \delta\Phi(s,t), \end{aligned} \tag{103}$$

where $s = z - ut$, and where $N(s), V(s)$ and $\Phi(s)$ satisfy the nonlinear traveling-wave equations (13)–(15), and $\delta N, \delta V$ and $\delta\Phi$ are perturbations to the wave. Substituting Eqs. (103) into Eqs. (6)–(8) and linearizing yields

$$\begin{aligned} &\frac{\partial}{\partial t}\delta N - u\frac{\partial}{\partial s}\delta N + \frac{\partial}{\partial s}(N\delta V + V\delta N) = 0, \\ &\frac{\partial}{\partial t}\delta V - u\frac{\partial}{\partial s}\delta V + \frac{\partial}{\partial s}(V\delta V) = -\frac{\partial}{\partial s}\delta\Phi, \\ &\frac{\partial^2}{\partial s^2}\delta\Phi - k_\perp^2\delta\Phi = -\delta N. \end{aligned} \tag{104}$$

We look for eigenmodes of these equations, with solutions behaving in time as $e^{-i\omega t}$, where ω is a (possibly complex) eigenfrequency associated with a given linear eigenmode. Also, we expand the eigenmodes in space in a Fourier decomposition of the same form as used in Eqs. (42)–(44)

$$\begin{aligned} \delta N(s,t) &= \Re e^{-i\omega t}\sum_{m=-\infty}^{\infty}\delta N_m e^{ims}, \\ \delta V(s,t) &= \Re e^{-i\omega t}\sum_{m=-\infty}^{\infty}\delta V_m e^{ims}. \end{aligned} \tag{105}$$

Since the coefficients in Equations (104) are real, the operation of taking the real part in Eqs. (105) can be stripped out of the equations. Then taking a Fourier component of the resulting equations yields

$$\begin{aligned} &-(\omega + um)\delta N_m + m\sum_{l=-\infty}^{\infty}(N_{m-l}\delta V_l + V_{m-l}\delta N_l) = 0, \\ &-(\omega + um)\delta V_m + m\sum_{l=-\infty}^{\infty}V_{m-l}\delta V_l = -\alpha_m\delta N_m, \end{aligned} \tag{106}$$

where N_m and V_m are Fourier coefficients of the nonlinear traveling wave, and δN_m and δV_m are Fourier coefficients of perturbations to the wave.

1. Three-wave theory

For nonlinear waves of small amplitude A, it is sufficient to consider only three waves in the stability analysis. If the nonlinear (pump) wave has wavenumber p, we consider its interaction with two other linear (daughter) waves of wavenumber l and m, respectively, that satisfy $p = l + m$. The pump wave is a single mode with nonzero Fourier amplitudes $\{N_p, V_p\} = \{N_{-p}, V_{-p}\} = \{A, uA\}$, where A is the amplitude (using the same notation as Sec. III B), and $u = \sqrt{\alpha_p/p}$ is the phase velocity of mode p (assuming small amplitude). Then, Eqs. (106) are reduced to four coupled equations for the daughter wave Fourier amplitudes

$$\begin{aligned} &-(\omega + um)\delta N_m + m(N_p\delta V_{-l} + V_p\delta N_{-l} + \delta V_m) = 0, \\ &-(\omega + um)\delta V_m + mV_p\delta V_{-l} = -\alpha_m\delta N_m, \\ &-(\omega - ul)\delta N_{-l} - l(N_{-p}\delta V_m + V_{-p}\delta N_m + \delta V_{-l}) = 0, \\ &-(\omega - ul)\delta V_{-l} - lV_{-p}\delta V_m = -\alpha_{-l}\delta N_{-l}. \end{aligned} \tag{107}$$

There is a second set of four equivalent equations involving $\{\delta N_{-m}, \delta V_{-m}\}$ and $\{\delta N_l, \delta V_l\}$, which can be obtained by interchanging the indices m and l in Eqs. (107). Equations (107) from a closed homogeneous set of linear equations which have a trivial solution $\delta N_m = \delta V_m = \delta N_{-l} = \delta V_{-l} = 0$,

but for special values of ω there is a nontrivial solution. It may be found by writing Eqs. (107) as the eigenvalue problem $\mathbf{A}\cdot\mathbf{Z}=\omega\mathbf{Z}$, where $\mathbf{Z}=(\delta N_m,\delta V_m,\delta N_{-l},\delta V_{-l})$, and the matrix $\mathbf{A}$ is

$$\mathbf{A}=\begin{pmatrix} -mu & m & muA & mA \\ \alpha_m & -mu & 0 & muA \\ -luA & -lA & lu & -l \\ 0 & -luA & -\alpha_l & lu \end{pmatrix}. \tag{108}$$

The eigenvalues ω of the matrix satisfy following polynomial equation:

$$\begin{aligned}&((\omega-lu)^2-\omega_l^2)((\omega+mu)^2-\omega_m^2)\\ &-A^2[2lmu^2(lu-\omega)(mu+\omega)+u(m\omega_l^2(3mu+2\omega)\\ &+l\omega_m^2(3lu-2\omega))+\omega_l^2\omega_m^2]+A^4l^2m^2u^4=0,\end{aligned} \tag{109}$$

where ω_l and ω_m are the frequencies of the daughter waves in linear theory (as seen in the lab frame): $\omega_l=\sqrt{l\alpha_l}$ and similarly for ω_m. The second set of four equivalent equations mentioned in relation to Eq. (107) leads to the same result as Eq. (109), but with l and m interchanged.

When there is no pump wave ($A=0$), Eq. (109) has four "unperturbed" solutions: $\omega=-mu\pm\omega_m$ and $\omega=lu\pm\omega_l$, which are frequencies of linear modes with wave numbers m and $-l$, respectively, traveling both to the left and to the right (when viewed in the lab frame), and Doppler-shifted by the pump wave phase velocity u since we are working in the pump wave frame of reference. To each eigenfrequency is associated an eigenvector $\mathbf{Z}=(\delta N_m,\delta V_m,\delta N_{-l},\delta V_{-l})$, which is the vector of density and velocity perturbations for that mode. For $\omega=-mu\pm\omega_m$, $\mathbf{Z}=(1,\pm\omega_m/m,0,0)$ while for $\omega=lu\pm\omega_l$, $\mathbf{Z}=(0,0,1,\mp\omega_l/l)$.

The addition of a nonzero pump wave amplitude A shifts the frequencies and mixes these unperturbed eigenvectors. The frequency shift of the daughter waves is similar to the nonlinear shift of the pump wave considered in Sec. III B, except that here the shift is of the daughter waves due to the pump, not a shift of the pump itself (which is neglected in this analysis).

When the pump wave amplitude A is small, Eq. (109) implies that the frequency shift of each eigenmode from its unperturbed value is also small (of order A^2), provided that none of the four daughter wave eigenfrequencies are degenerate. This scaling with amplitude agrees with the scaling found for nonlinear frequency shifts in Sec. III B. Also, the mixing of the eigenvectors is small; i.e., each eigenmode remains close to a daughter wave with a given wavenumber, with only a small admixture of the other daughter wave wavenumber. However, this changes if there is a near-degeneracy in the eigenfrequencies, and this degeneracy can produce strong mixing of the eigenvectors and an unstable eigenmode.

Degeneracies occur where $-mu\pm\omega_m=lu\pm\omega_l$. Recalling that $u=\omega_p/p$ where ω_p is the frequency of the pump wave, and that $p=l+m$, one finds degeneracy occurs when any of the following resonance conditions are met: $\omega_p=\omega_l+\omega_m,\omega_p=\omega_l-\omega_m$, or $\omega_p=\omega_m-\omega_l$ (assuming that ω_p,ω_l and ω_m are all positive). For our purposes, considering that the waves have nearly linear dispersion ($k_\perp>1$), only the first resonance condition can be satisfied. Then of the four eigenfrequencies, it is the two smaller frequency eigenmodes that are nearly degenerate: $\omega\approx-mu+\omega_m$ and $\omega\approx lu-\omega_l$. As seen in the lab frame, these two eigenmodes have nearly the same phase velocity as the pump wave if the dispersion is nearly linear. (The other two eigenmodes have phase velocities in the opposite direction as the pump when seen in the lab frame.) When the pump wave amplitude is zero, the unperturbed eigenvectors for these two near-degenerate eigenmodes are, respectively, $\mathbf{Z}=(1,\omega_m/m,0,0)\equiv\mathbf{Z}_1$ and $\mathbf{Z}=(0,0,1,\omega_l/l)\equiv\mathbf{Z}_2$.

Near degeneracy, we can use degenerate perturbation theory to describe the eigenmodes. The eigenmodes are a linear combination of $\mathbf{Z}_1$ and $\mathbf{Z}_2$

$$\mathbf{Z}=\alpha\mathbf{Z}_1+\beta\mathbf{Z}_2. \tag{110}$$

Thus, the perturbed density in an eigenmode has the form

$$\delta N(s,t)=\Re e^{-i\omega t}(\alpha e^{ims}+\beta e^{-ils}). \tag{111}$$

We then project the eigenvalue equation $\mathbf{A}\cdot\mathbf{Z}=\omega\mathbf{Z}$, with $\mathbf{Z}$ given by Eq. (110) and $\mathbf{A}$ by Eq. (108), onto $\mathbf{Z}_1$ and $\mathbf{Z}_2$, obtaining a reduced eigenvalue problem for α and β

$$\begin{aligned}\mathbf{Z}_1^\dagger\cdot\mathbf{A}\cdot\mathbf{Z}&=\omega\mathbf{Z}_1^\dagger\cdot\mathbf{Z},\\ \mathbf{Z}_2^\dagger\cdot\mathbf{A}\cdot\mathbf{Z}&=\omega\mathbf{Z}_2^\dagger\cdot\mathbf{Z},\end{aligned} \tag{112}$$

where the dagger denotes a left eigenvector: $\mathbf{Z}_1^\dagger=(\omega_m/m,1,0,0)$ and $\mathbf{Z}_2^\dagger=(0,0,\omega_l/l,1)$. Defining the detuning from resonance as

$$\Delta\omega=\omega_l+\omega_m-\omega_p, \tag{113}$$

defining the shift of the eigenfrequency from its value on resonance as

$$\delta\omega=\omega+mu-\omega_m, \tag{114}$$

and assuming both $\Delta\omega$ and $\delta\omega$ are of order the pump amplitude A (assumed small), the eigenvalue equation for α and β given by Eq. (112) is

$$\begin{pmatrix} 0 & A\dfrac{m\omega_l^2+2p\omega_l\omega_m+l\omega_m^2}{2p\omega_l} \\ -A\dfrac{m\omega_l^2+2p\omega_l\omega_m+l\omega_m^2}{2p\omega_m} & -\Delta\omega \end{pmatrix}\cdot\begin{pmatrix}\alpha\\ \beta\end{pmatrix}=\delta\omega\begin{pmatrix}\alpha\\ \beta\end{pmatrix}. \tag{115}$$

The two solutions for the eigenfrequency shift $\delta\omega$ are obtained from the quadratic equation

$$\delta\omega^2+\Delta\omega\delta\omega+A^2\frac{\left(m\omega_l^2+2p\omega_l\omega_m+l\omega_m^2\right)^2}{4p^2\omega_l\omega_m}=0, \tag{116}$$

which yields

$$\delta\omega = \frac{1}{2}\left(-\Delta\omega \pm \sqrt{\Delta\omega^2 - A^2\frac{\left(m\omega_l^2 + 2p\omega_l\omega_m + l\omega_m^2\right)^2}{p^2\omega_l\omega_m}}\right). \tag{117}$$

Equation (116) can also be obtained directly from Eq. (109) by assuming a degeneracy for which A, $\Delta\omega$, and $\delta\omega$ are all small and of the same order of magnitude.

For each solution, the coefficients α and β are related by

$$\delta\omega\alpha = A\frac{l\omega_m^2 + 2p\omega_l\omega_m + m\omega_l^2}{2p\omega_l}\beta, \tag{118}$$

implying that a near-degenerate eigenmode, with α and β of roughly the same size, is a strong admixture of daughter waves containing both wavenumbers l and m. From Eqs. (110), (114), and (113), the density perturbation for each eigenmode can be written as

$$\delta N(z,t) = \Re(\alpha e^{-i(\omega_m+\delta\omega)t+imz} + \beta e^{i(\omega_l-\delta\omega-\Delta\omega)t-ilz}), \tag{119}$$

where we used $s = z - ut$, $u = \omega_p/p$, and $p = l + m$. Note that $\omega_l - \delta\omega - \Delta\omega$ can also be written as $\omega_p - \omega_m - \delta\omega$. Thus, the sum of the two frequency components in the eigenmode equals ω_p. Physically, one frequency component in the density beats with the pump wave to produce the other frequency component, and vice versa; and therefore the frequency components add to the pump wave frequency ω_p.

When $A = 0$, from Eqs. (117) and (118), one eigenmode has $\delta\omega = 0$ and $\beta = 0$, while the other eigenmode has $\delta\omega = -\Delta\omega$ and $\alpha = 0$, i.e., each eigenmode is a single-wavenumber daughter wave, with frequency ω_m and ω_l, respectively, as seen in the lab frame (see Eq. (119)). As A increases from zero, the eigenmodes become a mixture of these daughter waves, each with a shifted frequency $\bar{\omega}_l$ and $\bar{\omega}_m$ given by

$$\bar{\omega}_l = \omega_l - \Delta\omega - \delta\omega^-,$$
$$\bar{\omega}_m = \omega_m + \delta\omega^+,$$

where $\delta\omega^\pm$ are the two solutions given by Eq. (116) with corresponding $\pm$ signs in the equation. (Here, and in what follows, we assume $\Delta\omega$ is a positive quantity, as is the case for linear dispersion relation given by Eq. (12).) These can be regarded as "natural" frequencies of the daughter waves in the presence of the pump wave. In other words, if one drives the three-wave system with an external potential proportional to $e^{imz-i\bar{\omega}_m t}$, one will obtain a large resonant response, and similarly for an external potential behaving as $e^{ilz-i\bar{\omega}_l t}$. However, a given eigenmode consists of one of these two daughter waves together with the other wave driven off of its natural frequency by an amount $\delta\omega^+ - \delta\omega^-$ (since a given eigenmode involves either $\delta\omega^-$ or $\delta\omega^+$, but not both; see Eq. (119)). The natural frequency of one daughter wave interacts with the pump to produce the other daughter wave at an off-resonant frequency.

The shifted natural frequencies are plotted schematically in Fig. 17 versus pump wave amplitude A. Each frequency is shifted downwards as the pump wave amplitude increases. If the amplitude becomes sufficiently large and if $\Delta\omega$ is sufficiently small, the sum of the two frequencies come into resonance with the pump wave frequency, and the three-wave system then becomes unstable.

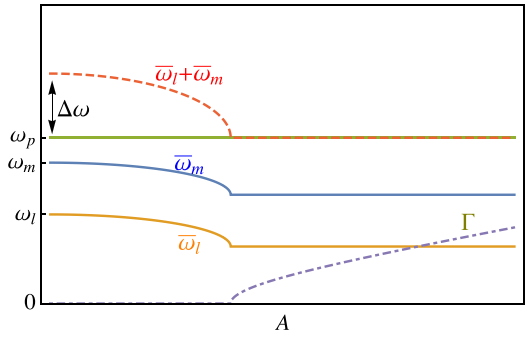

FIG. 17. Schematic of the real parts of the natural frequencies $\bar{\omega}_l$ and $\bar{\omega}_m$ for daughter waves l and m, respectively, versus pump wave amplitude A. Also shown is the pump wave frequency ω_p, which is independent of A in the three-wave model, as well as the sum of the daughter wave frequencies (dashed curve). When the pump amplitude is sufficiently large, this sum is shifted into resonance with the pump wave and instability results. The growth rate Γ is shown schematically as the dotted-dashed curve.

From Eq. (117), one can see immediately that exponential growth (or decay) of the daughter waves occurs when A satisfies

$$A > \frac{p|\Delta\omega|\sqrt{\omega_l\omega_m}}{m\omega_l^2 + 2p\omega_l\omega_m + l\omega_m^2}, \tag{120}$$

with a growth (or decay) rate Γ given by

$$\Gamma = \frac{1}{2}\sqrt{A^2\frac{\left(m\omega_l^2 + 2p\omega_l\omega_m + l\omega_m^2\right)^2}{p^2\omega_l\omega_m} - \Delta\omega^2}. \tag{121}$$

If one invokes nearly linear dispersion with $\omega_l \approx lu$ and $\omega_m \approx mu$, Eq. (121) simplifies further to

$$\Gamma = \frac{1}{2}\sqrt{9lmu^2A^2 - \Delta\omega^2}. \tag{122}$$

Physically, instability occurs because one daughter wave beats with the pump to produce a perturbation that resonantly drives the other daughter wave, and vice-versa. Even when the linear waves are not in perfect resonance (i.e., $\Delta\omega > 0$), the nonlinear frequency shift of the daughter waves pulls the waves into resonance with the pump wave; see Fig. 17 (an example of the well-known phenomenon of nonlinear frequency pulling and phase locking).

In the regime of small detuning, the growth rate is linear in the pump amplitude. According to Eq. (122)

$$\Gamma = 3\sqrt{lmu}A/2, \tag{123}$$

when $\Delta\omega \ll \Gamma$. This result is similar to the expression for the growth rate for the well-known modulational instability[23] for which the pump wavenumber p is assumed to be big compared to l. Then, daughter wave l can be thought of as a long wavelength modulation of the pump wave train, and the

growth rate of the modulation is, according to Ref. 23, $\Gamma_{mod} = \sqrt{-l^2\omega_p''\omega_2 A^2}$, where $\omega''_p = d^2\omega_p/dp^2$ and $\omega_2 A^2 = 3(k_\perp/p)^2 A^2\omega_p/4$ is the lowest order nonlinear frequency shift to the pump wave (see Eq. (68), and recall that this expression is for $p=1$, i.e., $k_\perp$ is normalized to p). Using Eq. (12) for ω_p, the expression for Γ_{mod} can be written as $\Gamma_{mod} = (3luA/2)k_\perp^2/\sqrt{k_\perp^2+p^2}$, which has the same scaling with A as Eq. (123). In the modulational instability, the daughter waves (i.e., modulations) are destabilized by the nonlinear frequency shift of the pump, whereas in the three-wave model used here the nonlinear frequency shifts are to the daughter waves and the shift to the pump is neglected.

Equation (123) shows that, for a given value of the pump wavenumber p, the daughter wave l with the maximum growth rate is the one with wavenumber $l = p/2$ (for even p values), since $m = p - l$. In what follows, we will therefore focus our attention on possible instabilities driven by a pump with $p=2$ and with daughter wavenumbers $l = m = 1$.

2. M wave theory

The previous three-wave analysis has the advantage of being both analytically tractable and intuitive. However, it leaves out several important effects. For instance, the nonlinear frequency shift of the pump wave is not included in the theory. Since this is an upward shift as amplitude A increases, one might then expect that nonlinear resonance between the pump and daughter waves would occur at smaller pump amplitude A than predicted by the three wave theory (see Fig. 17). However, another problem is that at finite amplitude A the pump wave is not a single mode; the nonlinear traveling wave has many Fourier components, all of which the three-wave theory neglects. Furthermore, these higher Fourier components become more intense as the detuning decreases. It is therefore unclear whether a three-wave analysis of nonlinear traveling waves that are of sufficiently large amplitude to be unstable has any validity.

In fact, we will see in the following analysis that three wave theory works to predict nonlinear frequency shifts of the daughter waves at very small amplitude, showing the expected downward shift in frequency, but does not work at larger amplitudes necessary for instability according to the three-wave theory. We find that if a sufficiently large number of modes are kept in the following analysis, no instability involving parametric decay to longer wavelength daughter waves can be identified, for *any* pump amplitude A.

We solve the eigenvalue problem given by Eqs. (106) numerically. We assume that only Fourier modes with wavenumbers of magnitude less than M for some (sufficiently large) value of M are required. As in the three-wave analysis, the set of Fourier coefficients of the density and velocity perturbations form a vector with $4M$ components, $\mathbf{Z} = (\delta N_{-M}, \delta V_{-M}, ..., \delta N_M, \delta V_M)$, (neglecting $\{\delta V_0, \delta N_0\} = \{0,0\}$) such that Eq. (106) can be considered a linear eigenvalue problem of the form $\mathbf{A}\cdot\mathbf{Z} = \omega\mathbf{Z}$. We therefore require the eigenvalues and eigenvectors of the matrix $\mathbf{A}$.

This numerical solution depends on an equilibrium solution for the Fourier coefficients N_m and V_m and the phase speed u of the nonlinear traveling wave for a given value of the transverse wavenumber $k_\perp$ and a given amplitude A. We calculate the equilibrium solution for a wave with fundamental wavenumber $p=1$ using the Fourier method described in Sec. III B, keeping $M+1$ Fourier mode pairs $\{N_m, V_m\}$ in the wave, with $-M/2 \le m \le M/2$, for amplitude A and transverse wavenumber $k_\perp/2$. We then transform this solution to one with fundamental wavenumber $p=2$ and with $2M+1$ Fourier mode pairs, via the scale transformation $m \to 2m$. The transformed wave has the same amplitude A and density components (i.e., $N_m \to N_{2m}$), but half the velocity (i.e., $u \to u/2$ and $V_m \to V_{2m}/2$) and twice the transverse wavenumber (i.e., $k_\perp/2 \to k_\perp$); and only the even Fourier components are nonzero. We make this transformation with the knowledge that a parametric resonance can now occur between the $p=2$ pump wave and longer wavelength $l = m = 1$ daughter waves.

For example, if we take $M=2$, we first set up a pump wave taking transverse wavenumber $k_\perp/2$ and keeping $M+1=3$ Fourier pairs, $\{\{N_{-1}, V_{-1}\}, \{N_0, V_0\}, \{N_1, V_1\}\}$, with $N_0 = 1, V_0 = 0, N_1 = N_{-1} = A$. This wave obeys the linear dispersion relation $u = \sqrt{\alpha_1} = 1/\sqrt{1+(k_\perp/2)^2}$, and $V_1 = V_{-1} = uA$. We then transform this to a wave with $2M+1=5$ Fourier pairs, with half the period and twice the transverse wavenumber, so that now $N_1 = N_{-1} = 0, V_1 = V_{-1} = 0, N_2 = N_{-2} = A, V_2 = V_{-2} = uA$ with $u = 1/\sqrt{2^2+k_\perp^2}$, which is half the speed of the untransformed wave. A solution of eigenvalue problem (106) then yields the same results as the three-wave analysis presented in Sec. V A 1. The pump wave with $p=2$ is unstable to parametric resonance with daughter waves $l = m = 1$ if the amplitude A exceeds the instability criterion given by Eq. (120). The frequency ω of the daughter waves as seen in the moving frame displays a downward frequency shift as in Fig. 17, and the frequency vanishes at instability (see Fig. 18), as expected from Eqs. (114) and (117) for

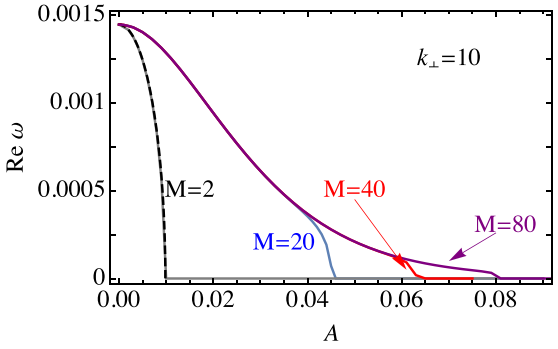

FIG. 18. The real part of the frequency ω (as seen in the frame of the pump wave) displays a downward frequency shift versus amplitude A for the lowest frequency eigenmode on a traveling pump wave with fundamental wavenumber $p=2$, transverse wavenumber $k_\perp = 10$, keeping M modes in the stability analysis, for $M = 2, 20, 40,$ and 80. For $M=2$, the frequency matches the prediction of three wave theory, Eqs. (117) and (114) (dashed line), for $l = m = 1, p = 2$. For larger M, the threshold amplitude beyond which the real frequency vanishes increases.

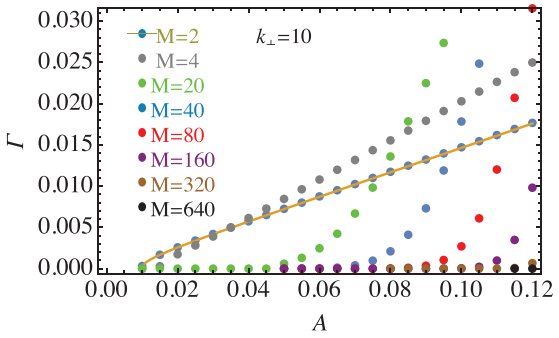

FIG. 19. The growth rate Γ for the unstable eigenmode on a nonlinear traveling pump wave with fundamental wavenumber $p=2$ versus the amplitude A of the traveling wave, keeping M modes in the stability analysis, and for $k_\perp = 10$. The $M=2$ case is compared to the prediction of three wave theory (the solid line), Eq. (122), with $l = m = 1$ and $p=2$.

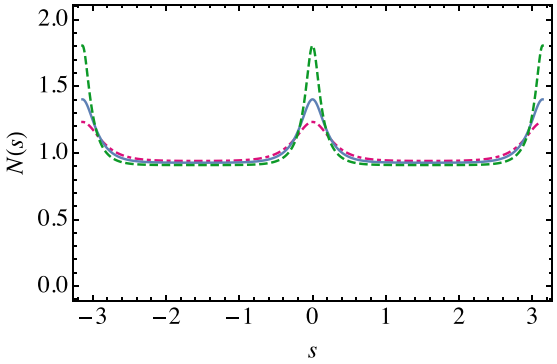

FIG. 21. Density versus position in a traveling wave with fundamental wavenumber $p=2$ and $k_\perp = 10$, for three amplitudes corresponding to the eigenmodes shown in Fig. 20: $A=0.05$ (dotted-dashed), $A=0.065$ (solid), and $A=0.085$ (dashed).

the case $l = m = p/2$. That is, in resonance, the daughter wave eigenmodes are stationary in the frame of the pump wave, but their amplitude grows or decays depending on the phase relation of the eigenmode to the pump. Just below threshold, the unstable eigenmode is a standing wave, oscillating slowly but not traveling (when viewed in the pump wave frame), with a frequency that approaches zero as the threshold is approached. This can be seen from Eqs. (118) and (117), which imply that at threshold $\alpha = -\beta$.

If one increases the value of M, for given amplitude A, one obtains a more accurate description of the nonlinear traveling wave, and the number of eigenmodes described by the system of equations also increases. We concentrate here on the low order eigenmodes with the slowest spatial variation. For sufficiently large values of M, these eigenmodes have converged spatial form and converged frequency ω that are independent of further increases in M. Among these slowly varying well-converged eigenmodes, for given values of A and M there is never more than one unstable mode. For $M=2$, the instability is the three-wave resonance described previously. For larger M, the instability appears to be a multi-wave version of the three-wave resonance. As for the three-wave case, as the amplitude A increases beyond a threshold value, two eigenmode frequencies approach zero (in the pump wave frame) and then become imaginary, one with positive imaginary frequency (a growing mode) and the other with negative imaginary frequency (a decaying mode). The real part of the frequency of these modes is shown in Fig. 18, and the imaginary part (the growth rate) is shown in Fig. 19. The spatial form of the unstable eigenmode is shown in Fig. 20 for three values of M, and for $k_\perp = 10$, at the value of A close to the instability threshold for that M value; in Fig. 21 the pump wave at these values of A is shown for reference. Just below the threshold value of A, these eigenmodes oscillate in place at a low frequency; they are standing waves when viewed in the pump wave frame, just as in the three wave case. The spatial form of the eigenmode is a derivative of the pump wave, along with a small distortion of the wave shape. In other words, this eigenmode is an oscillation of the two peaks of the nonlinear traveling wave toward and away from one-other, with a small distortion of the shape of the peaks. This is similar to a compressional wave on a chain of particles. For amplitudes just beyond instability, the shift in position of the two peaks grows exponentially as the peaks distort in shape.

It is not surprising that the frequency of such an eigenmode approaches zero at large amplitude. At large amplitudes, we have seen that the traveling wave becomes a series of sharp peaks similar to a train of solitons; see Fig. 21. These near-solitons are rather far apart with respect to their width, and thus interact only weakly with one another. Hence, their locations can be changed slightly with respect to one another without inducing much restoring force.

Note however, that the threshold value of the amplitude A necessary for instability increases as M increases; see Figs. 18 and 19. In fact, for sufficiently large M, all amplitudes A

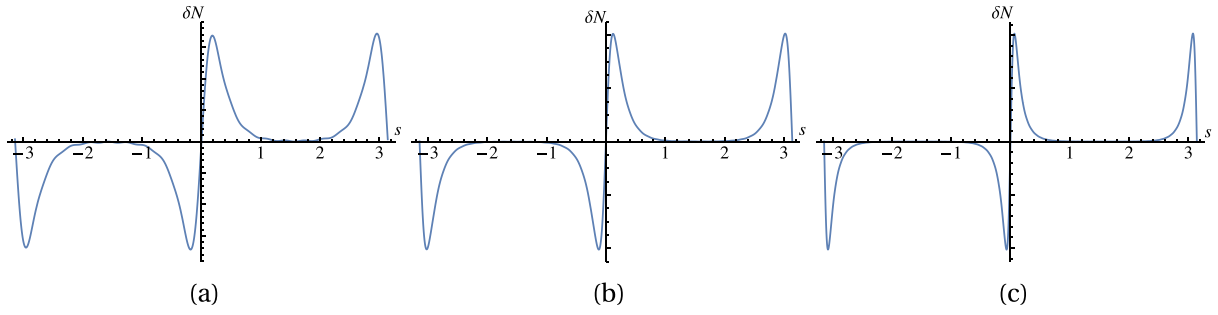

FIG. 20. The unstable density eigenmode near the lowest value of A for which instability occurs, for three values of M and for $k_\perp = 10$. (a) $M = 20, A = 0.05$, (b) $M = 40, A = 0.065$, and (c) $M = 80, A = 0.085$.

of physical relevance are stable. For $M=640$, the maximum value employed in our calculations, and for $k_\perp = 10$, the growth rate vanishes for A values up to $A=0.12$. This value of A corresponds to a maximum density in the wave of roughly 4.8, which is far beyond any experimentally relevant density for a nonlinear traveling TG wave.

While the results presented here are for $k_\perp = 10$, we find no qualitative difference with results for any other value of $k_\perp$ we have tested. For sufficiently large M, none of the well-converged eigenmodes are unstable; and the least stable (lowest frequency) eigenmodes have forms similar to those shown in Fig. 20.

Thus, we find that if the numerical resolution of a nonlinear traveling TG wave is sufficiently fine, the waves are linearly stable. The three-wave theory is not relevant to these waves because when $k_\perp > 1$ they contain many Fourier modes, obviating an analysis based on a small number of modes.

B. Standing waves

We now turn our attention to the linear stability of nonlinear standing waves. We consider linear perturbations to a nonlinear periodic standing wave that satisfies Eqs. (73)–(76). The perturbations satisfy linearized versions of Eqs. (73) and (74)

$$\delta\dot{N}_m(t) + \frac{m}{2}\sum_{m'=1}^{\infty}\{\delta V_{m'}[N_{m-m'} + N_{m'-m} - N_{m+m'}] + V_{m'}[\delta N_{m-m'} + \delta N_{m'-m} - \delta N_{m+m'}]\} = 0, \tag{124}$$

$$\delta\dot{V}_m(t) + \frac{1}{2}\sum_{m'=1}^{\infty} m'\{\delta V_{m'}[V_{m-m'} - V_{m'-m} + V_{m+m'}] + V_{m'}[\delta V_{m-m'} - \delta V_{m'-m} + \delta V_{m+m'}]\} = \alpha_m \delta N_m, \tag{125}$$

where $N_m(t)$ and $V_m(t)$ are the Fourier coefficients of the nonlinear standing wave, and $\delta N_m(t)$ and $\delta V_m(t)$ are the perturbed Fourier coefficients of the wave.

While these coupled ordinary differential equations are linear in the unknown functions δN_m and δV_m, the coefficients in the equations have periodic time dependence, which complicates their solution compared to the traveling-wave case. We first consider an analytic approach to the solution via two-timescale analysis applied to three waves, and then consider a numerical approach based on Floquet analysis for the general M waves case.

1. Three wave theory

For nonlinear standing waves of small amplitude A, it is sufficient to consider only three waves in the stability analysis. As in the traveling-wave case, let the nonlinear pump wave have wavenumber p and the two linear daughter waves have wave numbers l and m, where $p = l + m$. The pump wave again is described as a single Fourier mode with the following Fourier coefficients of a linear standing wave:

$$\{N_p(t), V_p(t)\} = A\{\cos(\omega_p t), (\omega_p/p)\sin(\omega_p t)\}, \tag{126}$$

where $\omega_p = \sqrt{p\alpha_p}$ is the frequency of the pump wave. Then Eqs. (124) and (125) reduce to

$$\delta\dot{N}_m(t) + \frac{m}{2}\left(-N_p(t)\delta V_l + V_p(t)\delta N_l + 2\delta V_m\right) = 0, \tag{127}$$

$$\delta\dot{V}_m(t) - \frac{m}{2}\left(V_p(t)\delta V_l\right) = \alpha_m \delta N_m, \tag{128}$$

together with equations for δN_l and δV_l that can be obtained from Eqs. (127) and (128) by interchanging l and m.

We will solve these equations approximately, assuming that the detuning $\Delta\omega$ given by Eq. (113) is small, of order A. Then a consistent solution has the form

$$\delta N_m(t) = n_m(\tau)e^{-i\omega_m t} + c.c., \tag{129}$$

$$\delta V_m(t) = v_m(\tau)e^{-i\omega_m t} + c.c., \tag{130}$$

and similarly for $\delta N_l, \delta V_l$, where $c.c.$ denotes complex conjugate, $\tau = At$ is a slow time variable, and $n_m(\tau)$ and $v_m(\tau)$ are slowly varying amplitudes for the daughter waves. Substituting these equations as well as Eq. (126) into Eqs. (127) and (128), we consider terms which vary in time like $e^{-i\omega_m t}$ and divide through by this factor, to obtain the following slow timescale equations:

$$-i\omega_m n_m + m v_m + A\frac{d}{d\tau}n_m - \frac{mA}{4}\left(v_l^* - \frac{i\omega_p}{p}n_l^*\right)e^{i\Delta\omega\tau/A} = 0, \tag{131}$$

$$-i\omega_m v_m - \alpha_m n_m + A\frac{d}{d\tau}v_m - \frac{imA\omega_p}{4p}v_l^* e^{i\Delta\omega\tau/A} = 0. \tag{132}$$

To zeroth order in A, these equations imply that $n_m = -imv_m/\omega_m$ and $\omega_m^2 = m\alpha_m$, which are the relations for linear waves. Similarly, one also has $n_l^* = ilv_l^*/\omega_l$ to lowest order in A (which follows from Eq. (131) with m and l interchanged). To first order in A, we may use these relations in the terms proportional to A in Eqs. (131) and (132). However, in the zeroth-order parts of the equations, we must keep a first-order correction, writing $n_m = -imv_m/\omega_m + A\Delta n_m$. Then, Eqs. (131) and (132) become

$$-i\omega_m A\Delta n_m - iA\frac{m}{\omega_m}\frac{d}{d\tau}v_m - \frac{mA}{4}v_l^*\left(1 + \frac{l\omega_p}{p\omega_l}\right)e^{i\Delta\omega\tau/A} = 0, \tag{133}$$

$$-\alpha_m A\Delta n_m + A\frac{d}{d\tau}v_m - \frac{imA\omega_p}{4p}v_l^* e^{i\Delta\omega\tau/A} = 0. \tag{134}$$

Then, multiplying Eq. (133) by $-i\omega_m/m$ and adding the result to Eq. (134) yield

$$-\left(\frac{\omega_m^2}{m} + \alpha_m\right)\Delta n_m + \frac{im}{4}v_l^*\left(\frac{\omega_m}{m} + \frac{l\omega_p\omega_m}{mp\omega_l} - \frac{\omega_p}{p}\right) = 0. \tag{135}$$

Substituting the solution of this equation for Δn_m into Eq. (134), and using the linear dispersion relation $\omega_m^2 = m\alpha_m$, then yields the slow time equation

$$\frac{d}{d\tau}v_m - i\gamma_l v_l^* e^{i\Delta\omega\tau/A} = 0, \tag{136}$$

where

$$\gamma_l = \frac{p\omega_l\omega_m + m\omega_l\omega_p + l\omega_m\omega_p}{8p\omega_l}. \tag{137}$$

Equation (136) is coupled to the slow-time equation for v_l, which is the same as Eq. (136) but with l and m interchanged

$$\frac{d}{d\tau}v_l - i\gamma_m v_m^* e^{i\Delta\omega\tau/A} = 0. \tag{138}$$

Writing $v_m(\tau) = (x_m(\tau) + iy_m(\tau))e^{i\Delta\omega\tau/2A}$, where x_m and y_m are real functions, and similarly for $v_l(\tau)$, we can convert Eqs. (136) and (138) into four coupled real ordinary differential equations for x_m, y_m, x_l, and y_l

$$\dot{x}_m(\tau) - \frac{\Delta\omega}{2A}y_m - \gamma_l y_l = 0, \tag{139}$$

$$\dot{y}_m(\tau) + \frac{\Delta\omega}{2A}x_m - \gamma_l x_l = 0, \tag{140}$$

$$\dot{x}_l(\tau) - \frac{\Delta\omega}{2A}y_l - \gamma_m y_m = 0, \tag{141}$$

$$\dot{y}_l(\tau) + \frac{\Delta\omega}{2A}x_l - \gamma_m x_m = 0. \tag{142}$$

Assuming that $x_m(\tau) = \Re x_{0m}e^{\Gamma_s\tau}$, and similarly for the other three unknown functions, allows determination of the slow timescale rate Γ_s from the determinant of the resulting matrix equation. The result is $\Gamma_s^2 = \gamma_l\gamma_m - \Delta\omega^2/(4A^2)$. Converting this variable to a fast-timescale rate $\Gamma = A\Gamma_s$ (i.e., writing x_m in terms of t rather than τ as $x_m = \Re x_{0m}e^{\Gamma t}$) then yields the growth (or decay) rate in the three wave theory

$$\Gamma = \frac{1}{2}\sqrt{4A^2\gamma_l\gamma_m - \Delta\omega^2}. \tag{143}$$

The rate is real provided that $4A^2\gamma_l\gamma_m > \Delta\omega^2$, otherwise the rate is imaginary and the daughter waves oscillate in amplitude rather than growing or decaying. This instability onset is similar to that found in the three wave theory for traveling waves, Eq. (120). When the dispersion is nearly linear with $\omega_m \approx um$ for all m, Eq. (143) simplifies to

$$\Gamma = \frac{1}{2}\sqrt{9A^2lmu^2/16 - \Delta\omega^2}, \tag{144}$$

which is identical to the traveling-wave growth (or decay) rate in the nearly linear dispersion regime, Eq. (122), except for a factor of 4 dividing A. This factor can be traced to the difference in the definition of A in the traveling and standing wave cases: for the traveling wave, the pump wave has the form $N_p = A\exp[i(pz - \omega_p t)] + c.c.$, whereas in the standing pump wave has the form $N_p = A\cos(pz)\cos(\omega_p t) = (A/4)\{\exp[i(pz - \omega_p t)] + \exp[i(pz + \omega_p t)]\} + c.c.$; so the standing pump wave is two counter-propagating traveling waves, each with amplitude $A/4$. Each traveling pump wave interacts with daughter waves with nearly the same phase velocity, and their interaction with the counter-propagating waves can be neglected in three-wave theory.

Thus, in the three-wave theory, the standing wave and its accompanying daughter waves can be treated as a superposition of essentially independent counter-propagating traveling waves, just as in linear theory. However, in the M-wave theory presented below, we will find that this is not true—the stability properties of a nonlinear standing wave differ from those of traveling waves.

2. M wave theory

We now solve Eqs. (124) and (125) for an arbitrary number of Fourier modes using a variant of Floquet theory. For a given nonlinear standing wave with amplitude A and frequency ω, we first assume that $\delta N_m = 0$ and $\delta V_m = 0$ for $m > M$, for some (sufficiently large) value of M. We then construct a vector of unknown Fourier coefficients $\mathbf{Z} = \{\delta N_1, \delta V_1, ..., \delta N_M, \delta V_M\}$, and note that Eqs. (124) and (125) can be expressed in vector form as $\dot{\mathbf{Z}} = \mathbf{A}(t)\cdot\mathbf{Z}$, where the matrix $\mathbf{A}(t)$ is periodic with period $T = 2\pi/\omega$. Now, consider a solution $\mathbf{Z}(t, \mathbf{Z}_0)$ of these differential equations for a given initial condition $\mathbf{Z}_0$. The homogeneous linear form of the differential equations implies that

$$\mathbf{Z}(t, \mathbf{Z}_0) = \mathbf{L}(t)\cdot\mathbf{Z}_0, \tag{145}$$

where the matrix $\mathbf{L}(t)$ is a linear transformation that takes the initial condition to the solution at time t. In particular, let us consider the solution integrated over one period T of the standing wave and define $\mathbf{Z}_1 = \mathbf{Z}(T, \mathbf{Z}_0)$. Then

$$\mathbf{Z}_1 = \mathbf{L}(T)\cdot\mathbf{Z}_0, \tag{146}$$

where the matrix $\mathbf{L}(T)$ has real coefficients. If we now integrate the differential equations starting at time $t = T$ with initial condition $\mathbf{Z}_1$ and ending one period later, at time $t = 2T$, at $\mathbf{Z}_2$, we will find that $\mathbf{Z}_2 = \mathbf{L}(T)\cdot\mathbf{Z}_1$ because the matrix $\mathbf{A}(t)$ is periodic and therefore has the same time dependence as in the previous integration. Proceeding to integrate n times, we find that

$$\mathbf{Z}_n = \mathbf{L}(T)^n\cdot\mathbf{Z}_0, \tag{147}$$

where $\mathbf{Z}_n = \mathbf{Z}(t = nT, \mathbf{Z}_0)$. Thus, stability of the system of equations is determined by the size of the eigenvalues λ of the matrix $\mathbf{L}(T)$. Any eigenvalue with magnitude greater than unity causes exponential growth in the solution. However, the product of the eigenvalues equals unity, because the equations of motion are conservative. Thus, any eigenvalue with magnitude greater than one must be balanced by eigenvalues with magnitudes less than one.

The accompanying eigenvector $\mathbf{Z}_{0j}$ to an eigenvalue λ_j with magnitude greater than one provides the functional form of the growing eigenmode at the instants of time $t = nT, n = 0, 1, 2, ...$ In between these times, the mode may have a quite complex time dependence, but returns to the form predicted by the eigenvector each period. Thus, the time dependence of the *jth* eigenmode $\mathbf{Z}_j(t)$ corresponding to eigenvector $\mathbf{Z}_{0j}$ has the following form:

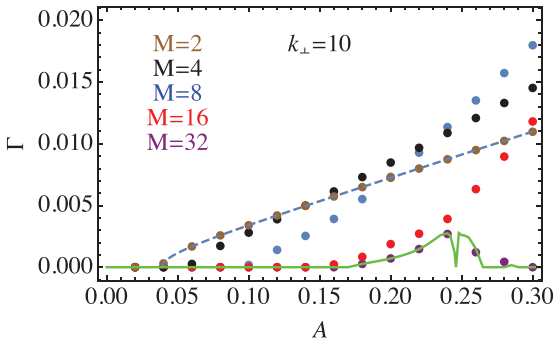

FIG. 22. Instability growth rate Γ for a standing wave with fundamental wavenumber $p=2$ versus amplitude A, for $k_\perp = 10$, and for increasing resolution of both the standing wave and the perturbations, from $M=2$ to $M=32$ (dots). Also shown is the growth rate predicted by three-wave theory taking $m = l = 1$ and $p=2$ in Eq. (143) (dashed), and the converged growth rate (solid) evaluated for M up to 120.

$$\mathbf{Z}_j(t) = \lambda_j^{t/T}\mathbf{Z}_{ej}(t), \tag{148}$$

where $\mathbf{Z}_{ej}(t)$ is a continuous (in time) periodic vector with period T that equals $\mathbf{Z}_{0j}$ at times $t = nT$. This vector can be written explicitly as $\mathbf{Z}_{e,j}(t) = \lambda_j^{\mathrm{Floor}(t/T)-t/T}\mathbf{L}(\mathrm{mod}(t,T))\cdot\mathbf{Z}_{0j}$, where $\mathrm{Floor}(x)$ is the integer nearest to but less than x.

In order to test the stability of a given standing wave, we determine the matrix $\mathbf{L}(T)$ by solving Eqs. (124) and (125) numerically over a single period T of the wave, for $2M$ different initial conditions. For the first initial condition, we take $\mathbf{Z}_0 = \{1,0,0,...\}$. The vector $\mathbf{Z}_1$ determined by the numerical integration of the equations provides us with the first column of the matrix $\mathbf{L}(T)$, according to Eq. (146). The next initial condition $\mathbf{Z}_0 = \{0,1,0,0,..\}$ determines the next column of $\mathbf{L}(T)$, and so on. Once we have found $\mathbf{L}(T)$ in this way, we evaluate the eigenvalues $\lambda_j, j = 1,..,2M$, to determine stability. The exponential growth rate Γ associated with an eigenvalue λ is then

$$\Gamma = \ln(|\lambda|)/T. \tag{149}$$

However, we limit ourselves to the set of eigenvalues that are well-converged, i.e., that do not vary with increasing M, for M sufficiently large. (Values of M up to 120 were employed.) Also, as for the traveling waves, we consider only standing waves with fundamental wavenumber $p=2$, for a range of amplitudes and for several $k_\perp$ values: $k_\perp = 4, 5, 6, 10$, and 20. We find that, among the converged eigenvalues, for a given amplitude A and value of $k_\perp$, either zero, one, or two eigenvalues have magnitudes larger than unity, and hence have nonzero growth rate Γ. When there is one such eigenvalue, it is real and negative, and the associated eigenvector $\mathbf{Z}_{0j}$ is also real. When there are two such eigenvalues, they are complex and are conjugate to one-another, and so are the eigenvectors. This implies that the growth rates for these two eigenvectors are identical.

In Fig. 22, we display numerical results for Γ versus the amplitude A of a standing wave with fundamental wavenumber $p=2$, $k_\perp = 10$, and for several values of M. The standing wave is also evaluated using M Fourier modes, using the methods of Sec. IV. Since its fundamental wavenumber is $p=2$, the standing wave has only even Fourier components. The unstable mode has only odd components.

For $M=2$, the calculated growth rate agrees with the rate given by three wave analysis, Eq. (143), taking daughter waves with $l = m = 1$ and a pump wave with $p=2$ (the dashed curve in the figure). For larger M, we observe a suppression of the growth rate similar to what was found for traveling waves. However, the converged growth rate found for sufficiently large M (the solid line) values does not vanish. While much reduced from the three wave theory, the growth rate remains finite for a range of A values.

Some of the growth rate values displayed in Fig. 22 correspond to a single real eigenmode with a negative eigenvalue, and others correspond to a complex-conjugate pair of eigenmodes with equal growth rates. The case of a single negative eigenvalue corresponds to a growing, oscillating perturbation which changes sign each period of the standing wave; i.e., a growing oscillation with exactly half the oscillation frequency of the standing wave, and phase-locked to the wave, just as for the three-wave theory. However, unlike three-wave theory, the functional form of the unstable eigenmode is not a single spatial Fourier mode. An example is displayed in Fig. 23 for $A=0.22$. The unstable density and velocity perturbation at the instant of maximum standing wave amplitude is displayed in (a), along with the standing wave at that instant, in (b). One period T later the perturbation changes sign and grows by the factor $|\lambda|$. An animation of the time dependence of the perturbation over two cycles

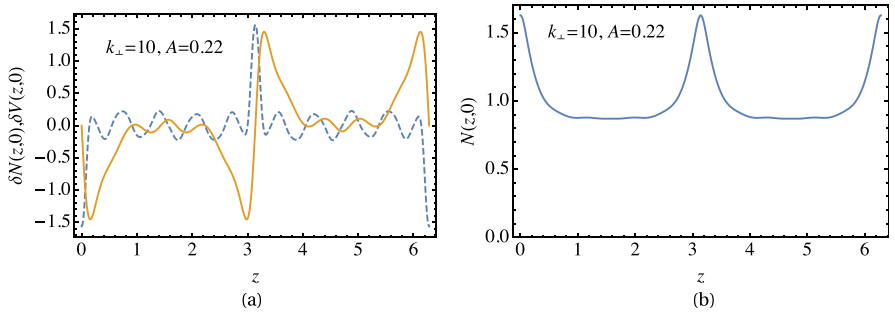

FIG. 23. (a) The unstable density eigenmode (dashed) and velocity eigenmode (solid) for a $p=2$ standing wave with $A=0.22$ and $k_\perp = 10$, at an instant of maximum amplitude of the wave. (b) The standing wave density at the same instant. Both evaluations were carried out for $M=80$. An animation of the perturbed density and the standing wave over two periods of the wave is supplied in the online material. (Multimedia view) [URL: http://dx.doi.org/10.1063/1.4932001.1]

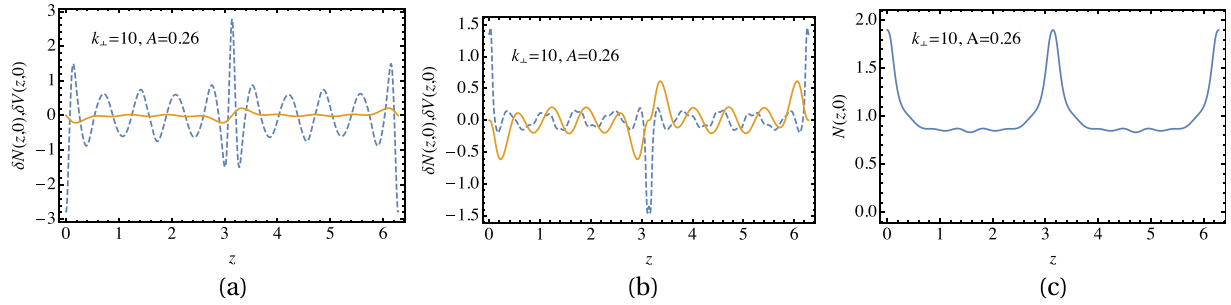

FIG. 24. The real (a) and imaginary part (b) of the unstable density eigenmodes (dashed) and velocity eigenmodes (solid) for a $p=2$ standing wave with $A=0.26$ and $k_\perp = 10$, at the instant of maximum amplitude of the wave. The growth rate for both eigenmodes is identical: $\Gamma = 1.498 \times 10^{-3}$ (see Fig. 22). (c) The standing wave density at the same instant. Evaluations were carried out for $M=120$.

of the standing wave can be found in the online material. These eigenfunctions are converged to within about one part in 10^{-3}. The spatial oscillations in the eigenmode are not artifacts of the finite number of Fourier modes kept in the expansion.

The functional form of the eigenmodes for a case for which there are two complex-conjugate unstable eigenvalues, $A=0.26$ and $k_\perp = 10$, is displayed in Fig. 24. The eigenvalues in this case are $\lambda = -1.03148 \pm 0.16398i$ and are well-converged to an accuracy of at least 10^{-5}. The two unstable complex-conjugate eigenmodes grow at the same rate. The unstable density and velocity perturbations at an instant of maximum standing wave amplitude are displayed in (a) and (b), corresponding to the real and imaginary parts, respectively, of the eigenvector for which $\Im\lambda > 0$. For the other unstable eigenvector, the real part (a) is the same and the imaginary part (b) has opposite sign. The standing wave at the same instant of maximum amplitude is displayed in (c). The real part of the eigenmode is somewhat similar in form to the case shown in Fig. 23. The imaginary part of the eigenmode is rather different in form (although its density perturbation may not be fully converged at our maximum resolution of $M=120$).

In Fig. 25, we display the converged growth rate of the unstable mode(s) versus standing wave amplitude for all values of $k_\perp$ studied. As $k_\perp$ decreases, the amplitude required for instability increases. Evidently, the larger dispersion of waves

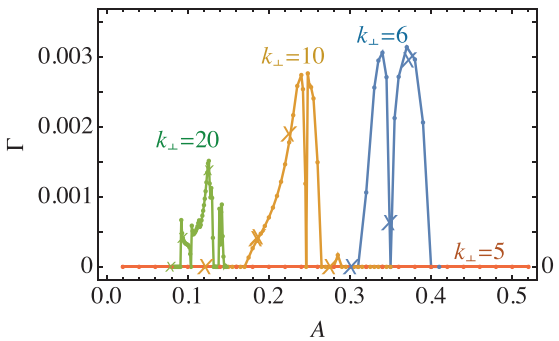

FIG. 25. Converged growth rate (dots connected by lines) versus amplitude A for standing waves with fundamental wavenumber $p=2$, and for several values of $k_\perp$. The X's are growth rates determined through simulation of the fluid equations, by adiabatically driving a standing wave to the given amplitude and seeding it with a small $m=1$ Fourier mode.

with smaller $k_\perp$ increases the amplitude required for mode coupling and instability. This is expected even in the three wave theory, but the required amplitude we observe is considerably larger than three wave theory would predict.

For example, for $k_\perp = 5$ or less, no instability in converged eigenmodes is observed, up to the maximum amplitude tested, $A = 0.52$, corresponding to a maximum density at $k_\perp = 5$ of $N_{\max} = 3.8$ (the onset of instability at $k_\perp = 5$ is predicted by three-wave theory to be at $A=0.14$; see Eq. (144)). For $k_\perp = 6$, there is a single unstable eigenmode for amplitudes in the range $0.32 < A < 0.34$ (the first peak), while for larger A values (the second peak) there are two complex-conjugate unstable eigenmodes. For $k_\perp = 10$, there is a single unstable eigenmode for amplitudes in the range $0.17 < A < 0.25$ (the first peak), while for larger A values there are two unstable complex-conjugate eigenmodes. For $k_\perp = 20$, the growth rate results have a rather complicated structure. There is a single unstable eigenmode for amplitudes in the ranges $0.092 < A < 0.127$ and $0.139 < A < 0.14$, and there are two complex-conjugate unstable modes in the ranges $0.128 < A < 0.131$ and $0.141 < A < 0.145$. We emphasize that this complicated structure is not the result of numerical noise; the growth rates are well converged for all amplitude values shown. Some of the structure can be associated with the previously discussed jumps in the density of the standing wave. For instance, the first appearance of unstable modes at $A=0.092$ occurs at the leftmost density jump shown in Fig. 13 (recall that the $p=1, k_\perp = 10$ standing wave considered in Fig. 13 can be mapped by a scale transformation to the $p=2, k_\perp = 20$ wave considered in Fig. 25).

In Fig. 26, we display the growth rates versus the scaled amplitude $3uA/4\Delta\omega$, which in three-wave theory equals unity at the instability onset for all $k_\perp \gg 1$ (see Eq. (144)). One can see that as $k_\perp$ increases, the scaled amplitude required for instability increases as well. This is because as $k_\perp$ increases, the dispersion becomes more linear at a given amplitude so there is more mode-coupling that increases the harmonic content of both the standing wave and the growing eigenmode, making 3 wave theory a less-relevant approximation.

We have tested these results by simulating the full nonlinear fluid equations, Eqs. (6)–(8). Details of the simulation method are described in Appendix B. In one set of simulations, we begin the simulation with a standing wave with fundamental wavenumber $p=2$ at a given amplitude, to

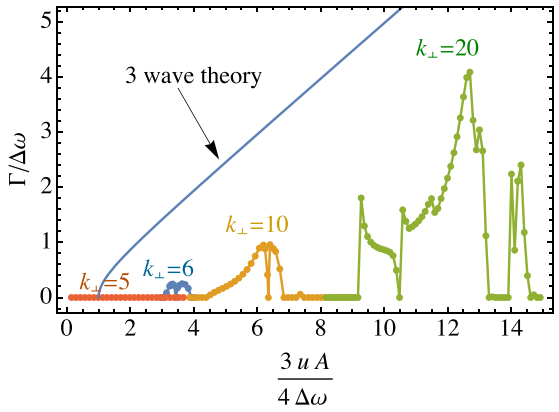

FIG. 26. Converged growth rate (dots connected by lines) versus scaled amplitude $3uA/4\Delta\omega$ for standing waves with fundamental wavenumber $p=2$, and for several values of $k_\perp$. The solid line shows the prediction of three-wave theory, Eq. (144) taking $l=m=1$ and $p=2$.

which a small "seed" density perturbation is added. This initial density perturbation has only $m=1$, i.e., it varies initially as $\cos(z)$. Instability of the system is measured by evaluating the rate of growth of the $m=1$ Fourier amplitude of the density. An example growth-rate measurement is shown in Fig. 27(a). Agreement of the growth rate evaluated in this way with the previously described Floquet analysis is typically better than one percent. About half of the points shown in Fig. 25 were evaluated using this simulation method.

One can see in Fig. 27(a) that eventually the growth of the perturbation saturates and there follows a complicated nonlinear "bouncing" of the perturbation amplitude. This nonlinear saturation behavior can be described analytically in three-wave theory,[24] but there is no good description for the M-wave case aside from simulation results such as these.

For cases where there are two complex-conjugate unstable eigenvalues, the initial condition overlaps with both eigenmodes and both grow up at the same rate. Beating between these two eigenmodes is then observed in the $m=1$ Fourier amplitude (see Fig. 27(b)). However, the exponential growth rate can still be picked out and it matches well to the previous Floquet analysis.

In a second set of simulations, we start with an equilibrium plasma and drive a standing wave to a given amplitude by forcing the system with an external time-dependent potential. This was described in Sec. IV, and details of the driving potential function can be found in Appendix B. The external potential is a single Fourier mode in time and space, with frequency close to ω_2, but with a slowly varying Gaussian envelope in time. To the resulting standing $m=2$ wave, we then add a small seed density with $m=1$ and again evaluate the rate of growth of the $m=1$ Fourier amplitude. Growth rates determined in this manner are shown with x's in Fig. 25. These growth rates also agree fairly well with the Floquet analysis.

VI. DISCUSSION

In this paper, we have explored some of the consequences of weak dispersion for the nonlinear behavior of $k_\perp \gg 1$ Trivelpiece-Gould plasma waves. We observed that strong mode coupling induced by weak dispersion in standing TG waves caused nonlinear resonances with the wave's own harmonics, that in turn induced jumps in the waveform at particular wave amplitudes. At these amplitudes, a single harmonic in the wave satisfied the linear dispersion relation and was therefore driven to large amplitude itself. This type of nonlinear resonance might also be apparent in other weakly dispersive nonlinear systems such as nonlinear shallow water waves, or sound waves, or ion sound waves, but we have not found evidence of this phenomenon reported in the literature.

We did not observe this resonance phenomenon in traveling TG waves. Such resonances would require $m=n$ (see Eq. (79)) because space and time dependence are related through the single variable $s=z-ut$. In other words, the phase velocity of the nonlinear wave would have to match the phase velocity of a linear wave whose wavenumber is a multiple of the fundamental wavenumber of the nonlinear wave. This cannot happen for TG waves because the nonlinear phase velocity is an increasing function of amplitude but the linear phase velocity is a decreasing function of wavenumber, so the linear phase velocity of a spatial harmonic can never match the nonlinear phase velocity.

However, for a nonlinear system whose phase velocity increases (or decreases) *both* with amplitude and wavenumber, such degeneracies could occur and nonlinear resonances of a traveling wave with its own harmonics are then possible.

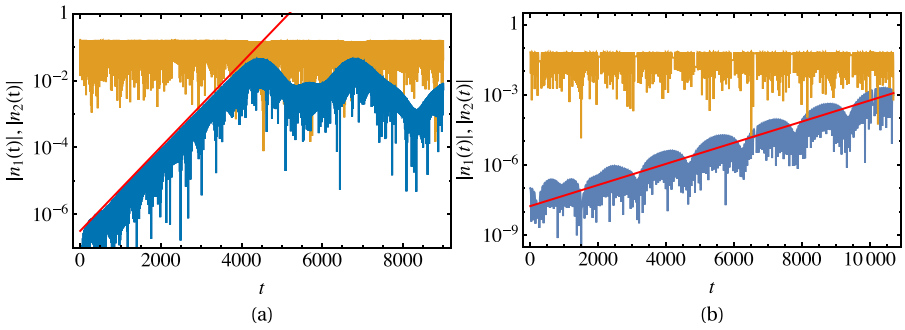

FIG. 27. The growth rate measured in nonlinear simulations of the fluid equations. The magnitude of the Fourier components $n_1(t)$ and $n_2(t)$ in the simulation are displayed, along with an exponential fit to $n_1(t)$. The simulation keeps M Fourier modes. (a) $k_\perp=6, A=1/3, M=48$. The instability grows until it saturates, but one can fit to the exponential part of the growth (solid line). (b) $k_\perp=20, A=0.13, M=80$. Beats in $n_1(t)$ are due to interference between the two unstable eigenmodes.

Certain optical systems are of this type; for example, an optical system with refractive index that increases with frequency and with amplitude (through the optical Kerr effect). Harmonic generation in these systems could make use of such resonances. In particular, for optical frequency-doubling, resonance occurs when the "phase-matching" requirement

$$\mathcal{N}(2\omega,0)=\mathcal{N}(\omega,A),$$

is met, where $\mathcal{N}(\omega,A)$ is the frequency-and-intensity-dependent refractive index of a nonlinear medium through which the light travels (and here A is the intensity of a beam of frequency ω that is to be frequency-doubled in the nonlinear medium). [This phase-matching requirement is equivalent to the condition that the phase velocity of the frequency-doubled wave matches that of the fundamental.] Nonlinearity of the refractive index could then be used to produce strong harmonic generation by satisfying this resonance condition with a high intensity pump wave.

However, the intensity dependence of the index is typically too weak to be of much importance in the resonance condition (at the intensities of interest in most applications), so that the linear refractive index $\mathcal{N}(\omega,0)$ is a good approximation for the right side of the equation.[25] In this case, the phase-matching requirement is satisfied using other effects, such as birefringence, or periodic poling, in an anisotropic medium such as a uniaxial crystal.[26]

We observed that mode coupling in TG waves reduced instability of the waves due to parametric resonance. For traveling waves, instability is completely suppressed, while for standing waves, the amplitude threshold necessary for instability onset is several times the prediction of three-wave theory (depending on $k_\perp$), and the growth rate is smaller.

One important aspect of the stability calculations presented here is that, in order to obtain converged growth rates, a great many Fourier harmonics had to be included in the calculations, especially at larger amplitudes. However, the cold fluid theory we have used could be a poor approximation for the higher harmonics, depending on parameters not included in the theory such as temperature or viscosity. In experiments that observe parametric instability in TG modes, such high harmonics could be Landau-damped, damped through collisions, or shifted in their resonant frequency by finite thermal pressure or finite plasma radius effects. A more realistic theory, incorporating these effects, will probably be needed to make contact with current experiments, since the wave dynamics is apparently quite sensitive to the number of harmonics that actually participate.

In addition, the use of Neumann boundary conditions for the wave potential is problematic for large amplitude standing waves in the current experiments on finite length plasmas, as this approximation neglects the motion of the plasma ends, which has an important influence on the reflection of the waves.

ACKNOWLEDGMENTS

The authors benefited from useful discussions with Professor T. O'Neil, Professor C. F. Driscoll, and Professor H. Milchberg; Dr. F. Anderegg and Dr. John Bollinger; and Matt Affolter. The research was supported by National Science Foundation Grant No. PHY-1414570, and Department of Energy Grant Nos. DE-SC0002451 and DE-SC0008693.

APPENDIX A: THE $k_\perp=0$ CASE: COLD LANGMUIR WAVES

The $k_\perp=0$ limit of Eqs. (6)–(8) admits a general analytic solution in Lagrangian coordinates. Equations (6) and (7) can be written as

$$\frac{dN}{dt}=-N\frac{\partial V}{\partial z}, \tag{A1}$$

$$\frac{dV}{dt}=-\frac{\partial\Phi}{\partial z}, \tag{A2}$$

where the total time derivative along a Lagrangian trajectory is $d/dt=\partial/\partial t+V\partial/\partial z$. Introducing the inverse density variable $U=1/N$, and taking a second total time derivative of Eq. (A1), yields

$$\frac{d^2U}{dt^2}=U\left(\frac{\partial V}{\partial z}\right)^2+U\frac{d}{dt}\frac{\partial V}{\partial z}. \tag{A3}$$

However, the derivatives in the last term in Eq. (A3) can be exchanged

$$\begin{aligned}\frac{d}{dt}\frac{\partial V}{\partial z}&=\frac{\partial^2V}{\partial t\partial z}+V\frac{\partial^2V}{\partial z^2}\\&=\frac{\partial}{\partial z}\frac{dV}{dt}-\left(\frac{\partial V}{\partial z}\right)^2.\end{aligned} \tag{A4}$$

When Eq. (A4) is substituted in Eq. (A3), and Eq. (A2) is employed, the result is

$$\begin{aligned}\frac{d^2U}{dt^2}&=-U\frac{\partial^2\Phi}{\partial z^2}\\&=1-U,\end{aligned} \tag{A5}$$

where in the last step Eq. (8) was applied, taking $k_\perp=0$. Equation (A5) is a harmonic oscillator equation with solution $U=1+C\cos(t+\psi)$, where C and ψ are constants of integration that depend on the initial conditions (i.e., they are functions of the initial position z_0 of a fluid element).

Thus, in the Lagrangian picture, the density oscillates with unit frequency (that is, at the plasma frequency), independent of the spatial form or amplitude of the initial conditions as given by $C(z_0)$ and $\psi(z_0)$ (which determine the initial density and velocity fields). (Note that an arbitrary constant velocity can be added to the velocity field, which causes a Doppler shift to the oscillation frequency that is not apparent in Eq. (A5) because this equation is valid in the frame of the fluid flow.) However, this solution is valid only provided that the characteristics $z(z_0,t)$ do not cross, which requires $|C|<1$; otherwise the density and velocity field become ill-defined. [The characteristics can be found by solving $dz/dt=V(z,t)$ with initial condition $z=z_0$.] Thus, provided that oscillation amplitudes are small enough so that

$|C| < 1$, all solutions of the $k_\perp = 0$ cold fluid equations simply oscillate at the plasma frequency, independent of their spatial form.

APPENDIX B: SIMULATION OF THE FLUID EQUATIONS

Numerical solutions to Eqs. (6)–(8) were evaluated using the Galerkin method, by expanding the density, velocity, and potential in spatial Fourier modes

$$N(z,t) = \sum_{m=-M}^{M} n_m(t) e^{imz},$$
$$V(z,t) = \sum_{m=-M}^{M} v_m(t) e^{imz}, \tag{B1}$$
$$\Phi(z,t) = \sum_{m=-M}^{M} \phi_m(t) e^{imz},$$

dropping Fourier coefficients for $|m| > M$, and taking $n_0(t) = 1, \phi_0(t) = v_0(t) = 0$. Reality of the density implies that $n_{-m}(t) = n_m^*(t)$, and similarly for the velocity and potential. Using this Fourier expansion, Eqs. (6)–(8) become coupled ordinary differential equations for the Fourier coefficients

$$\dot{n}_m(t) + im \sum_{l=-M}^{M} n_l(t) v_{m-l}(t) = 0, \tag{B2}$$

$$\dot{v}_m(t) + i \sum_{l=-M}^{M} l v_l(t) v_{m-l}(t) = -i\alpha_m n_m(t). \tag{B3}$$

Equations (B2) and (B3) can then be integrated for given initial conditions, for $1 \le m \le M$. Depending on the initial conditions, either traveling waves or standing waves can be simulated using these equations. For example, for standing waves, we choose initial conditions with $n_m(0)$ real and $v_m(0)$ imaginary. The form of the equations then guarantees that $n_m(t)$ will remain real and $v_m(t)$ will remain imaginary for all t, and the reality conditions then imply that $n_{-m}(t) = n_m(t)$ and $v_{-m}(t) = -v_m(t)$ so that the density has a cosine Fourier expansion and the velocity a sine expansion, as in Eqs. (69) and (70).

In some simulations, we drive the system with an external potential in order to produce a nonlinear standing wave. In this case, we modify Eq. (B3) to read

$$\dot{v}_m(t) + i \sum_{l=-M}^{M} l v_l(t) v_{m-l}(t) = -i\alpha_m n_m(t) - im\phi_{\mathrm{ext}_m}(t), \tag{B4}$$

where $\phi_{\mathrm{ext}_m}(t)$ is the Fourier coefficient of the external potential. This mimics experiments that create standing waves in the plasma column by driving a potential on external electrodes surrounding the plasma. In order to drive a standing wave with fundamental wavenumber p, we take the following form for this potential:

$$\phi_{\mathrm{ext}_m}(t) = \epsilon e^{-(t-t_0)^2/\Delta t^2} \sin(\Omega t) \delta_{m,p}. \tag{B5}$$

TABLE I. Parameters in some simulations of driven standing waves.

$k_\perp$	ϵ	Ω	Δt	M	A
6	1.5×10^{-4}	$1.0009\omega_2$	158	24	0.302
6	1.5×10^{-4}	$1.04\omega_2$	158	24	0.348
6	1.6×10^{-4}	$1.04\omega_2$	158	24	0.373
10	5×10^{-5}	$1.05\omega_2$	180	24	0.187
10	6.5×10^{-5}	$1.06\omega_2$	208	24	0.225
10	8.25×10^{-5}	$1.065\omega_2$	208	30	0.276
20	1.5×10^{-6}	$1.017\omega_2$	2247	36	0.079
20	3.5×10^{-6}	$1.022\omega_2$	1004	40	0.094
20	1.275×10^{-5}	$1.065\omega_2$	1297	40	0.126

The frequency Ω is chosen at, or slightly above, the linear frequency of the fundamental mode, and the time Δt is chosen so that $\Omega \Delta t \gg 1$, so that the wave is driven to large amplitude adiabatically. This allows time for all of the harmonics in the standing wave to couple to the fundamental. The time t_0 is chosen to be greater than $3\Delta t$. The amplitude parameter ϵ along with Δt determine the ultimate size of the resulting standing wave. There is an art to choosing these parameters. If Δt is too large, the wave will be driven up and then back down as nonlinearity changes the response of the system to the forcing. If Δt is too small, the resulting wave will not have the correct harmonic content for a standing wave of the given amplitude. The resulting wave is also sensitive to the value of Ω, particularly at larger amplitudes. Table I shows the values of parameters used in some of the simulations of $p = 2$ standing waves, as well as the amplitude A of the resulting wave.

These standing waves can then be seeded with a small amplitude $m = 1$ Fourier mode in order to test stability. The growth rates resulting from such tests are displayed as the X's in Fig. 25.

[1] A. W. Trivelpiece and R. W. Gould, J. Appl. Phys. **30**, 1784 (1959).
[2] J. H. Malmberg and C. B. Wharton, Phys. Rev. Lett. **17**, 175 (1966).
[3] W. M. Mannheimer, Phys. Fluids **12**, 2426 (1969).
[4] J. P. Lynov, P. Michelsen, H. L. Pecseli, J. Juul Rasmussen, K. Saeki, and V. A. Turikov, Phys. Scr. **20**, 328 (1979).
[5] H. Schamel, Phys. Scr. **20**, 336 (1979).
[6] F. Anderegg, M. Affolter, A. Ashourvan, D. H. E. Dubin, F. Valentini, and C. F. Driscoll, "Nonlinear plasma wave decay to longer wavelength," AIP Conf. Proc. Vol. 1668, edited by H. Himura, A. Sanpei, and Y. Soga (AIP Publishing, Melville NY, 2015) p. 020001.
[7] H. Higaki, Plasma Phys. Controlled Fusion **39**, 1793 (1997).
[8] E. Infeld and G. Rowlands, Proc. R. Soc. London **366**, 537 (1979).
[9] G. B. Whitham, *Linear and Nonlinear Waves* (John Wiley and Sons, New York, 1974) Sec. 13.11.
[10] G. B. Whitham, *Linear and Nonlinear Waves* (John Wiley and Sons, New York, 1974), p. 468.
[11] H. Ikezi, P. J. Barrett, R. B. White, and A. Y. Wong, Phys. Fluids **14**, 1997 (1971).
[12] D. F. DuBois and M. V. Goldman, Phys. Rev. Lett. **14**, 544 (1965).
[13] K. Nishikawa, Phys. Soc. Jpn. **24**, 916 (1968).
[14] V. P. Silin, Zh. Eksp. Teor. Fiz. **48**, 1679 (1965).
[15] V. N. Oraevskii and R. Z. Sagdeev, Zh. Tekh. Fiz. **32**, 1291 (1962).
[16] S. A. Prasad and T. M. ONeil, Phys. Fluids **22**, 278 (1979).
[17] J. K. Jennings, R. L. Spencer, and K. C. Hansen, Phys. Plasmas **2**, 2630 (1995).
[18] J. R. Danielson, D. H. E. Dubin, R. G. Greaves, and C. M. Surko, Rev. Mod. Phys. **87**, 247 (2015).
[19] G. B. Whitham, *Linear and Nonlinear Waves* (John Wiley and Sons, New York, 1974), p. 462.

[20]E. Infeld, P. Frycz, and T. Czerwinska-Lenkowska, Lett. Nuovo Cimento **44**, 537 (1985).
[21]R. Z. Sagdeev, D. A. Usikov, and G. M. Zaslavsky, *Nonlinear Physics—From the Pendulum to Turbulence and Chaos* (Harwood Academic, New York, 1988), p. 25.
[22]V. E. Zakharov, "Collapse and self-focussing of Langmuir waves," in *Basic Plasma Physics*, edited by A. A. Galeev and R. N. Sudan (North-Holland, Amsterdam, 1984), Vol. II, Chap. 5.3.
[23]G. B. Whitham, *Linear and Nonlinear Waves* (John Wiley and Sons, New York, 1974), p. 489.
[24]R. Z. Sagdeev and A. A. Galeev, *Nonlinear Plasma Theory* (W. A. Benjamin, New York, 1969).
[25]R. Boyd, *Nonlinear Optics*, 3rd ed. (Academic Press, Boston, 2008), Eq. (2.3.5).
[26]R. Boyd, *Nonlinear Optics*, 3rd ed. (Academic Press, Boston, 2008), Secs. 2.3 and 2.4.